LAWRENCE
LIVERMORE
NATIONAL
LABORATORY

UCRL-JRNL-215632

Silicon-Germanium Films Deposited by Low Frequency PE CVD: Effect of H2 and Ar Dilution

A. Kosarev, A. Torres, Y. Hernandez, R. Ambrosio, C. Zuniga, T. E. Felter, R. R. Asomoza, Y. Kudriavtsev , R. Silva-Gonzalez, E. Gomez-Barojas, A. Ilinski, A. S. Abramov

September 23, 2005

Journal of the Materials Research Society

JMR-2004-0903 accepted to J.Mat.Res.

Silicon-Germanium Films Deposited by Low Frequency PE CVD: Effect of H_2 and Ar Dilution

A.Kosarev [1], A.Torres [1], Y.Hernandez [1], R.Ambrosio[1], C.Zuniga [1] T.E.Felter[2], R.Asomoza[3], Y.Kudriavtsev[3], R.Silva-Gonzalez[4], E.Gomez-Barojas[5], A.Ilinski[6], A.S.Abramov [7]

[1]Institute National for Astrophysics, Optics and Electronics, INAOE, Apdo.Postal.51-216, CP 7200, Puebla, Mexico
[2]Lawrence Livermore National Laboratory, Livermore, CA, 94550, USA
[3]CINVESTAV-IPN, Av.IPN #2508, Mexico, D.F. 07360
[4]Instituto de Fisica, Benemerita Universidad Autonoma de Puebla, Apdo.Postal J-48, Puebla, Pue., C.P. 72570, Mexico
[5]CIDS-IC, Benemerita Universidad Autonoma de Puebla, Apdo.Postal 1651, Puebla, Pue. C.P.72000, Mexico
[6] Benemerita Universidad Autonoma de Puebla, Puebla, Puebla 72050, Mexico[7]A.F.Ioffe Phys.-Technical Institute, St.-Petersburg, 194021, Russia

Abstract

We have studied structure and electrical properties of $Si_{1-Y}Ge_Y$:H films deposited by low frequency PE CVD over the entire composition range from Y=0 to Y=1. The deposition rate of the films and their structural and electrical properties were measured for various ratios of the germane/silane feed gases and with and without dilution by Ar and by H_2. Structure and composition was studied by Auger electron spectroscopy (AES), secondary ion mass spectroscopy (SIMS) and Fourier transform infrared (FTIR) spectroscopy. Surface morphology was characterized by atomic force microscopy (AFM). We found: 1. The deposition rate increased with Y maximizing at Y=1 without dilution. 2. The relative rate of Ge and Si incorporation is affected by dilution. 3. Hydrogen preferentially bonds to silicon. 4. Hydrogen content decreases for increasing Y. In addition, optical measurements showed that as Y goes for 0 to 1, the Fermi level moves from mid gap to the conduction band edge, *i.e.* the films become more n-type. No correlation was found between the pre-exponential and the activation energy of conductivity. The behavior of the conductivity γ-factor suggests a local minimum in the density of states at E≈0.33 eV for the films grown with or without H-dilution and E≈0.25 eV for the films with Ar dilution.

PACS codes: 81.15.Gh; 68.55.-a; 78.30.-j

Corresponding author:
Andrey Kosarev
Address: INAOE, L.E.Erro #1, Box Puebla 72000, Mexico
Phone: 52-22-266 31 00 ext. 1409, Fax: 52-22-266 81 34, E-mail: akosarev@inaoep.mx

1. Introduction

Silicon-germanium alloys ($Si_{1-Y}Ge_Y$:H) are used as a low-bandgap material in multi-junction amorphous silicon solar cells [1-3] and are of much interest for other applications, e.g. un-cooled micro-bolometers [3-4] and in un-cooled bolometers [5-7].

Jordan *et al.* [8] have very recently studied a nano-crystalline Ge p-i-n structure. Despite implementation in device structures, $Si_{1-Y}Ge_Y$:H films have been significantly less studied and their electronic properties are poorly understood in comparison to those for amorphous silicon. Reviews of earlier work on $Si_{1-Y}Ge_Y$:H films can be found in refs. [9,10]. Although radio frequency (f = 13.56 MHz) plasma enhanced chemical vapor deposition (RF PECVD) remains the major technique for fabrication of $Si_{1-Y}Ge_Y$:H films, alternative methods, such as electron-cyclotron resonance (ECR) plasma deposition [11] and non-plasma hot wire (HW) deposition [12], have also demonstrated promising results. Dalal *et al.* [13] have found a positive role of ion bombardment on film growth and electronic properties of $Si_{1-Y}Ge_Y$:H films. With this in mind, a low frequency (LF) capacitive discharge, which has thicker near electrode sheathes [14], could provide increased ion bombardment. Nevertheless, only one paper, Budagian *et al.* [15], reports LF PECVD deposition of $Si_{1-Y}Ge_Y$:H films. Although the various investigations have found that the optoelectronic properties of these films change significantly with deposition conditions, it seems that all these methods of alloying Si with Ge result in deterioration of the photo-electronic properties. Most of the publications deal with relatively low Ge concentration ($Y < 0.5$) and only these films have provided opto-electronic properties suitable for application in device structures. The investigation of $Si_{1-Y}Ge_Y$:H films over the entire range $0 \leq Y \leq 1$ has been reported in refs. [16-18]. Feed gases (SiH_4, GeH_4 or GeF_4) have been mixed with the dilution gas Ar [19], He [17] or H_2 [20]. The latter is of great importance for fabrication of micro- [21] and nano- crystalline films [22, 23]. Nevertheless, the effect of dilution gas on both film growth and electronic properties has not been systematically studied.

The present report concerns an investigation of growth, structural, optical and electrical properties of $Si_{1-Y}Ge_Y$:H films over the entire range of Ge concentrations $0 \leq Y \leq 1$ in films deposited by LF PE CVD from silane-germane mixtures with and without argon and hydrogen gas dilution.

2. Experiment

The samples of amorphous silicon germanium films were prepared by LF PECVD decomposition using a modernized PECVD system from Applied Materials Inc., Model 3300. Silane, SiH_4, and germane, GeH_4, were used as the feed gases and hydrogen and argon as the dilution gases. Two different substrates were used: "Corning 1737" glass for the conductivity measurements and crystalline silicon (c-Si) for the measurements of infrared spectra. The films were deposited at substrate temperature T_s = 300C. The deposition parameters were as follows: pressure, P = 0.6 Torr; power, W = 350 W; and frequency f = 110 kHz. The total flow of silane and germane, $Q_{SiH4,GeH4}$, was 50 sccm and for all depositions. Three types of the samples were fabricated, 20:1 hydrogen dilution (H-dilution), 10:1 argon dilution (Ar-dilution), and without dilution. Prior to film growth on glass substrates, stripes of aluminum electrodes with 1-2 mm inter-electrode distance were deposited by e-beam evaporation. For pure germanium samples, *i.e.* Y = 1, a silicon nitride layer was deposited after film growth in order to protect the sample and avoid oxidation. The germane content in the gas phase X, defined as the gas flow ratio $X=Q_{GeH4}/Q_{SiH4+GeH4}$, was varied from 0 to 1. The thickness of the films was measured by a Dektak II step profiler. Composition of the films was characterized by secondary ion mass spectroscopy (SIMS) and Auger electron spectroscopy (AES). SIMS profiles were measured with a Cameca IMS-6f ion microprobe. Sputtering during SIMS utilized a cesium ion beam with primary ion energy from 5 to 15 keV. The primary ion beam was raster scanned approximately 200 microns, and the secondary ions emitted from a central area of 60 microns were monitored after mass and energy separation with an electron multiplier.

We monitored negative secondary ions to check contaminants H, C, O, and N. The solid solution composition was analyzed with a special mode in which secondary ions CsM^+ (where M is the analyzed element) were monitored during cesium sputtering. Oxygen flooding was always used with this mode in order to minimize the SIMS matrix effect found in SiGe compounds. We deposited a thin gold film on the surface of samples prone to charging and applied an electron beam charge compensation technique during the SIMS analysis.

The AES data were obtained by means of a JEOL system, Model JAMP-7800, with hemispherical electrostatic Auger energy analyzer. The system operates in ultra-high vacuum ($\geq 10^{-8}$ Pa) with energy resolution of 0.6% to 0.06%. The Auger spectra were recorded using a 10 keV electron beam at $5x10^{-8}$ A after the samples were sputtered clean by an Ar^{+} ion beam with kinetic energy of 3 keV and rastered over a 20x35 μm^2 area. The Si(LVV), N(KLL), Ge(LMM), and Si(KLL) transitions were observed in the Auger spectra. The Si(KLL) line was used for semi-quantified analysis of the concentration as discussed in Sect. 3.2.

Atomic force microscopy (AFM) was employed to study surface morphology of the films. These measurements were conducted with a Quesant Scanning Probe Microscope. Hydrogen bonding in the films was studied by Fourier transform infrared (FTIR) spectroscopy. The IR absorption spectra of the films were measured with a Brucker infrared spectrometer, Model Vector-22 over the range 350 to 4000 cm^{-1}. The measured transmission spectra were normalized to the transmission spectrum of a crystalline silicon substrate, and the absorption coefficient was determined by the Brodsky-Cardona-Cuomo method [24].

The spectral dependence of the optical absorption coefficient $\alpha(h\nu)$ was calculated from optical transmission $T(h\nu)$ measurements by the method described in refs. [25, 26]. $T(h\nu)$ was measured with a Perkin Elmer spectrophotometer Model Lambda 3B. Optical constants, namely the refractive index, n, and the extinction coefficient k were determined at $\lambda = 0.63$ μm by variable angle ellipsometry (VAR) using a EL X-02 C ellipsometer. The conductivity of the films was measured in the DC regime in a vacuum thermostat with bias voltage $U_b = 40$ V. The temperature dependence of conductivity was measured with the heating-cooling rate of approximately 1deg/min.

3. Results

3.1. Film growth

Depending on gas dilutor, we observed different deposition rates of the films for X ranging from 0 (pure Si) to 1 (pure Ge). The deposition rate was measured by dividing the

film thickness by deposition time. Fig. 1 shows the dependence of deposition rate, V_d, on germanium content in the film for the three cases, hydrogen dilution, argon dilution and without dilution. At low Ge-content, X = 0.1, the highest rate, V_d= 2.5 A/s, was observed in the films deposited with Ar dilution and the lowest rate, V_d= 1.5 A/s, in the films deposited with H-dilution. In all cases, V_d increases with Ge content but the detailed form of $V_d = f(X)$ depends on gas-dilutor. In samples fabricated without dilution, V_d increased with X and reached the maximum rate of 3.7 A/s at X = 1. With H-dilution, V_d initially increased rapidly, then more slowly to a maximum of 2.8 A/s again at X=1. With Ar dilution, V_d first decreases, reaching a minimum at X = 0.2, and then slowly increases to 3 A/s at X = 1. The growth of these $Si_{1-Y}Ge_Y$:H films will be discussed in Section 4 and compared with the literature.

3.2. Composition characterization

SIMS profiling and Auger spectroscopy (AES) were employed to characterize the composition of the films. SIMS profiles are shown in Fig. 2 for representative samples deposited with hydrogen dilution. In our analysis we use only the values of the concentrations determined in the middle part of the film excluding interface regions. The absolute values of Si and Ge concentrations were obtained assuming the concentration of Si atoms is $N_{Si} = 5x10^{22}$ atoms/cm^3 in the pure Si substrate and the concentration of Ge atoms is $N_{Ge} = 4.4x10^{22}$ atoms/cm^3 in the pure Ge films. The "peaking" of Si and Ge at the interfaces is caused by the SIMS matrix effect. We analyzed the film composition in the CsM^+ mode with oxygen flooding. The result obtained was compared with the AES measurements and with SIMS measurements of negative Si and Ge ions using relative sensitivity factors (RSF)

for a Si matrix. We analyzed C, H, and O as negative atomic ions, whereas nitrogen was analyzed as SiN^- and GeN^- molecular ions. The concentration of these elements (C, H, N and O) was estimated with RSFs obtained for implanted Si standards. The incorporation of Ge, Si, H and O atoms was studied in the films prepared with different germane feed gas contents (X) and with different dilutions. The efficiency of Ge incorporation is of great importance and seldom reported in the literature. Fig. 3 shows the Ge-content in our films defined as $Y = N_{Ge}/(N_{Ge}+N_{Si})$ as a function of Ge content in the feed gas, X. The experimental points obtained by both SIMS (filled symbols) and AES (corresponding unfilled symbols) are presented. They are in agreement within 10%. Some of the discrepancy is related to different probe depths; AES is more sensitive to the surface (sub-surface) region than the SIMS signal obtained from a region near mid-thickness. The incorporation of hydrogen and oxygen in our films will be discussed together with IR data in Section 3.5.

3.4. AFM characterization

Surface morphology of the films was characterized by AFM. AFM images (with dimensions 2x2μm) were taken for randomly selected parts of the sample. Statistical analysis of the surface roughness of the images was performed for the AFM images described by the function of height distribution Z(x,y). Height histograms were plotted and the following characteristics were determined: average height, $\langle Z \rangle$, average roughness, R_a, standard deviation of Z-height (root mean square, RMS), R_q, and correlation length L_c. Determination of these characteristics are described e.g. in [27]. These characteristics are listed in Table 1. We can see from Table 1 that roughness, measured as R_q, and as R_a, changed with Ge content, X, Y and these changes depend on the dilution used. In the films deposited with H-

dilution, roughness R_a (R_q) increases from 0.6(0.8) to 3.1(4.0) nm as Y increases from 0.42 to 0.0.87. In the films deposited with Ar dilution, no significant change was observed as Y goes from 0.23 to 0.90. In the films obtained without dilution, roughness R_a (R_q) increases from 0.6(0.8) to 13(15) nm with Y for Y=0.33 to 0.79. Correlation length showed more complex behavior with Y: growth of L_c from 42 (Y=0.33) to 149 nm (Y=0.79) in the films deposited without dilution; minimum L_c=40 nm at Y=0.60 in the films deposited with Ar dilution, and maximum L_c=95 nm at Y=0.62 in the films obtained with hydrogen dilution.

3.5. IR spectra

General views of IR spectra for the $Si_{1-Y}Ge_Y$:H samples are shown in Fig.4 (a) for X = 0, 0.1 and (b) for X = 1. The spectra contain lines corresponding to stretching modes at approximately 2000 cm^{-1} for Si-H and 1880 cm^{-1} for Ge-H bonds. The rocking and wagging deformation modes are seen at approximately 640 cm^{-1} for Si-H and 560 cm^{-1} for Ge-H. The mode at 1950-2000 cm^{-1} can also be related to the absorption of the stretching mode of Ge-H and to Ge-H_2 bonds located on surfaces, e.g. on surfaces of voids as reported by Comedi *et al.* [28]. In this case, however, this line should exist in a-Ge:H films, which has not been observed in the films studied, see Fig. 4b. Therefore we assign the absorption at 2000 cm^{-1} to Si-H bonding because it was observed only in films that contained Si atoms.

The absorption related to Si-O and Ge-O bonds was observed in the range of 990 - 1100 cm^{-1} and 690-840 cm^{-1} respectively. Lukovsky *et al.* [29] have assigned absorption at 860 - 870 cm^{-1} to the Ge-O-Ge stretching mode resulting from oxygen incorporation during plasma growth. The vibrational mode at 960 cm^{-1} was observed in almost all Si-Ge films, but it could not be unambiguously assigned. This line has been observed in previous IR spectra

but was not assigned [30]. It has been reported earlier by Lukovsky *et al.* [31, 32] that absorption bands at 650 cm^{-1} and 940 cm^{-1} appeared in oxygen doped a-Si:H films. The position of the lines, k_0, their widths, w, and areas, S, obtained after analyzing the spectra are listed in Table 2.

The concentration of chemical bonds, e.g. Si-H, can be determined from the area of the corresponding line either for stretching or for deformation mode by means of the equation:

$$N_{Si-H} = A\int_{-\infty}^{+\infty}\frac{\alpha(k)}{k}dk \approx \frac{A}{k_O}\times S, [cm^{-3}] \quad \ldots\ldots\ldots\ldots\ldots\ldots \quad (1)$$

where A is a constant determined from other experiments (e.g. hydrogen effusion [33, 34] nuclear reaction analysis [35], nuclear magnetic resonance [36] etc.), $\alpha(k)$ is the spectral dependence of the IR absorption in the vicinity of the line at $k=k_0$ and S is the area under the corresponding line.

Then, assuming that all hydrogen is chemically bonded e.g. with Si in a-Si-H films it is possible to calculate the hydrogen concentration

$$C_H = \frac{N_{Si-H}}{\rho}\times 100, [at.\%] \quad \ldots\ldots\ldots\ldots\ldots\ldots \quad (2)$$

where ρ is atomic density in atoms/cm^3.

There is little data in the literature regarding the A-values for stretching and deformation modes in Si-H bonds [25, 33, 37-39] and even less in Ge-H bonds [33, 37, 38]. It should also be noted that A-values for films deposited by different techniques and by different laboratories can vary. This makes it difficult to calculate H-concentration using IR data and A-values from the literature. Nevertheless, we have estimated C_H using formulas (1)

and (2) and substituting $A_{Si\text{-}Hstr}$ (2000) = $9x10^{19}cm^{-2}$ [39], $A_{Si\text{-}Hdef}$ (630)=$2.1x10^{19}cm^{-2}$ [39] and $A_{Ge\text{-}Hstr}$ (1880)= $5x10^{19}cm^{-2}$ [37] in order to reveal trends in C_H with increasing Ge-content in the film and with dilution in the feed gas. Relative errors in the estimations are determined by the errors related with calculation of S in eq. (1), which are less than 1%. This is acceptable for comparative analysis. Errors in absolute values of hydrogen concentration are mainly determined by A constants.

Fig. 5 shows H-content, C_H, as a function of Ge-content, Y, in the films. Generally, C_H reduces with increasing Y. The minimum value of C_H occurs at $C_H \approx 1$ at.% for Ge films (Y=1) and is achieved in the films deposited without dilution. Films deposited with either H- or Ar-dilution had approximately twice the hydrogen content, $C_H \approx 2$ at.%. At low Ge content (Y=0.1), the highest values of hydrogen content are $C_H \approx 5.5$ at.% and are observed for films deposited with H-dilution.

It is interesting to compare the behavior of C_H determined by both FTIR and SIMS with the Ge content, Y, in the film. Both data show a similar general trend: C_H reduces with increasing Ge. FTIR and SIMS data demonstrate good agreement in the range of Y = 0.5 to 1.0. For low Ge content, Y=0.1-0.5, the two methods disagree by approximately a factor of 2.

In a similar way, using the absorption line in the region $850 < k < 1050$ cm^{-1}, we estimate the oxygen content C_O in the films by substituting the corresponding A-value: A = 0.156 at%/eVcm^{-1}[38]. Note, we use this value for both Si-O and Ge-O bonds because, to our knowledge, the A-constant for Ge-O bonds has not been reported. The behavior of C_O determined by both FTIR and SIMS *vs.* Y is shown in Fig.6. All films showed O-content reducing with Y increasing. The discrepancy, however, between the C_O values determined by

FTIR and by SIMS was typically a factor of two to four. The lowest O-content was observed by both techniques at Y = 1 *i.e.* for pure a-Ge films. Nelson *et al.* [40] have also reported a decrease of the oxygen concentration as measured by SIMS with Y for Y > 0.5 without reporting a mechanism or reason for this behavior. As known for a-Si:H films, there should be some quantity of hydrogen that optimally terminates dangling bonds in the $Si_{1-Y}Ge_Y$:H films and therefore achieves the best electronic properties. We could also expect some optimal distribution of this hydrogen between the Si and Ge atoms since the sensitivity of electronic properties to dangling bonds need not be the same for Si and Ge atoms. The problem of hydrogen distribution between Si and Ge atoms in Si-Ge films has been discussed in refs.[41-43], but the optimum concentration has not yet been reported in the literature.

In order to characterize the hydrogen distribution in the films studied we use a parameter called "Ge-H preference" $P_{Ge-H} = \left(\frac{S_{Ge-H}}{S_{Si-H}}\right) / \left(\frac{Y}{1-Y}\right)$, where Y is the Ge content in the film and S_{Ge-H} and S_{Si-H} are the areas of the absorption lines corresponding to the stretching mode of Ge-H and Si-H bonds, respectively. P = 1 corresponds to a proportional distribution of hydrogen between Si and Ge atoms. P < 1 reflects that Ge atoms are under-terminated by hydrogen and there are extra Ge dangling bonds. P > 1 indicates that there are extra Si dangling bonds. P_{Ge-H} values calculated from the IR data are as follows: P_{Ge-H} = 0.45±02, 0.61±0.04 and 0.29±0.04, for the films deposited with hydrogen, argon and without dilution, respectively. We have observed only $P_{Ge-H} < 1$. This suggests that hydrogen is not evenly distributed between the Ge and Si atoms in Si-Ge films. The distribution, *i.e.* the exact value of P_{Ge-H}, depends on the dilution gas mixture during growth.

3.6. Optical absorption measurements

3.6.1. Spectral dependence of optical absorption

The spectral dependence of the optical absorption coefficient $\alpha(h\nu)$ is shown in Fig.7(a) for all the samples studied along with that for a-Si for comparison. As can be seen, $\alpha(h\nu)$ curves shift to lower photon energy with increasing Ge content in the feed gas. The total shift is about 0.9 eV when Y changes from 0 to 1. The shift is not proportional to Y; nearly half of the total shift occurs in the low Y region between Y = 0 and Y=0.42. The effect of dilution is rather pronounced for Y = 0.23 –0.6; the films deposited with H-dilution are shifted more than the others.

In order to determine the optical band gap, E_g, we follow the method of Tauc. Thus, the $\alpha(h\nu)$ curves are re-plotted as $\sqrt{\alpha h\nu} = f(h\nu)$, Fig.7 (b), and the optical parameters are determined from the best fit of the experimental points to the equation

$$\sqrt{\alpha h\nu} = B(h\nu - E_g) \quad \ldots\ldots\ldots\ldots\ldots\ldots\ldots\ldots \quad (3)$$

Additionally we determine the photon energies E_{03} and E_{04} as those providing absorption coefficients $\alpha = 10^3$ and $\alpha = 10^4$ cm^{-1}, respectively. Their difference, $\Delta E = E_{04} - E_{03}$, characterizes the slope of $\alpha(h\nu)$. The optical characteristics discussed above are listed in Table 3. The B-factor can be calculated from the band tail density of states using the equation $B^2 = (4\pi\sigma_{min})/(nc\Delta E_w)$, where σ_{min}, n, c, and ΔE_w are the minimal conductivity, the refractive index, the velocity of light, and the width of the band gap, respectively [44]. The determination of the optical gap from experimental data for non-crystalline materials is not as unambiguous as for crystalline materials and Tauc plot determinations are therefore supplemented or even replaced by considerations of the characteristic photon energy E_{04}. In

our opinion, it is better to use the difference $\Delta E = E_{04} - E_{03}$ than ΔE_w for characterizing the band tail states because it is extracted from the region of $\alpha = 10^3 - 10^4$ cm^{-1}, which is typical for band tail related absorption. Thus, ΔE reflects the steepness of the convolution of the conduction band tail and valence band tail density of states. ΔE_w, on the other hand, is calculated through the B factor obtained from the best fit of the Tauc plot at $\alpha > 10^4$ cm^{-1}, *i.e.* the region typical for band-to-band absorption. The experimental values of E_{04}, E_{03}, ΔE and ΔE_w are listed in Table 3. Fig. 8 shows the behavior of ΔE *vs.* Y to depend on the dilution used. The films deposited with H- or Ar-dilution exhibit a maximum of ΔE at $Y \approx 0.6$ that suggests an increased density of states in the band tails. The films deposited without dilution demonstrate a minimum at $Y \approx 0.45$ and further growth of the density of states in the band tail at higher Y.

3.6.2. Optical constants obtained by variable angle ellipsometry

Additional optical characterization of the films was obtained by variable angle ellipsometry, VAE, which determines the optical constants n (the refractive index) and k (the extinction coefficient). Ellipsometric angles Δ and Ψ were measured at several (11-13) angles with 1° steps in the vicinity of the quasi Bruster angle at the incident laser beam wavelength $\lambda = 0.63$ μm. Using the values for the film thickness and the optical constants for the substrate previously measured, we determined the optical constants of each film that best fit the measured Δ and Ψ values for all angles of the incident laser beam. This was performed with the MAELS code developed by Dr. A. Selkin (Ioffe Phys.-Technical Inst., St-Petersburg, Russia) because it provided a better fit and higher accuracy than that supplied

by the instrument manufacturer. The optical characteristics measured by VAE are listed in Table 4. The refractive index, n, significantly increases with the addition of germane to the feed gas. In particular, $n \approx 3.92$ for a-Si:H; $n \approx 5.44$ to 5.47 at $X = 0.1$, and $n \approx 5.74$ to 6 at $X = 1$. By comparison, the optical constants at $\lambda = 0.63$ μm for crystalline Ge range from $n = 5.588$ and $k = 0.933$ [45] to $n = 5.64$ and $k = 0.8$ [46]. Thus, the refractive index, n, obtained for the films with $X \geq 0.2$ ($Y \geq 0.45$) are close to the values for c-Ge. For $X = 1$ ($Y = 1$), *i.e.* the germanium films, a thin SiN protecting film was used. All other measured samples had no SiN coating. The Si-N layer protecting was not incorporated in the optical model and this simplified two layer optical model may explain why the refractive index in the pure Ge films is measured to be higher than that in c-Ge.

The simplified two layer optical model, or perhaps oxygen in the surface of the film, also lowered the value of k from crystalline germanium. The behavior of k with X is complex without a clear trend. However, when the values of k are used to calculate the absorption coefficient, α, using $\alpha = 4\pi k/\lambda$, a systematic increase in α *vs.* Y is apparent, see Fig. 9. The figure also shows a similar trend for α *vs.* Y, when calculated from the spectral dependence of transmission. For both measurement techniques, α(Y) increases linearly with Y and with the same slope. The values for α from VAE are shifted downward compared to those from the transmission technique. This could be due to different sensitivities of the techniques to volume and surface properties. Transmission measurements sense absorption in the volume, while ellipsometry is very sensitive to surface properties. The offset in the curves in Fig. 9 could arise from oxide and pores at the surface which would decrease the value for the surface sensitive technique, VAE.

3.7. Conductivity measurements

Electrical properties of the films were studied by measurement of the temperature dependence of the conductivity, σ(T). Fig. 10 shows σ(T) curves for the samples plotted as logσ *vs.* 1/T. The experimental curves can be described by activation dependence

$$\sigma(T) = \sigma_0 \exp(-Ea/kT) \quad \text{..... (4)}$$

where E_a *i*s the activation energy determined from the slope of the experimental curves logσ vs. 1/T. The temperature dependence of E_C and E_F can be written as [47]

$$E_C(T)-E_F(T)= E_C(0)-E_F(0) -\gamma T \quad \text{.....(5)}$$

Where $E_C(T)$ and $E_F(T)$ are the positions of conduction band edge and Fermi level at temperature T and γ is the temperature coefficient. The theoretical temperature dependence of the conductivity can be written as

$$\sigma(T) = \sigma_{\min} \exp(\gamma / k) \exp[(E_C(0) - E_V(0)) / kT] \quad \text{…….. (6)}$$

where it is conventionally accepted σ_{min} = 200-300 $Ohm^{-1}cm^{-1}$ [47].

From comparison of (4) and (6) the values determined experimentally are

$$\sigma_0 = \sigma_{min}\exp(\gamma/k) \quad \text{.....(7)}$$

and $E_a = E_C(0)-E_F(0)$ .....(8)

The transport characteristics extracted from the σ(T) data are listed in Table 5. From the data presented in this table and in Fig.10, we can see that Ge incorporation significantly changes conductivity of the films. Room temperature conductivity increases from $\sigma_{RT} = 2x10^{-8}$ at Y= 0 to $2x10^{-1}$ $Ohm^{-1}cm^{-1}$ at Y = 1, *i.e.* by 7 orders of magnitude. The activation energy changes from E_a = 0.60 at Y = 0 to 0.22 eV at Y = 1, *i.e.* by nearly a factor of 3. Except for the case, Y = 1, H-dilution lowers, sometimes substantially, the values of the activation energy in

comparison to films deposited with or without Ar-dilution. The effect of Ar-dilution was small compared to the non-diluted case except at Y≈0.9-1.0 for the γ-factor temperature dependence, column 8, Table 5.

It is interesting to compare the behavior of the optical gap, $E_g(Y)$, and the Fermi level at room temperature, $E_F^{RT}(Y)$, *vs.* the Ge-content, Y. The corresponding curves plotted in Fig. 11 clearly show both optical gap and Fermi position decreasing with increasing Ge-content. The solid lines are the result of a computer generated best fit and demonstrate that in both the cases the behavior can be roughly described by a linear dependence:

$E_g(Y) = 1.7 - 0.7Y \quad (R_{Eg} = 0.93)$ ……(9)

$E_F^{RT}(Y) = 0.73 - 0.42Y \quad (R_{Ef} = 0.91)$ ……...(10)

Where R_{Eg} and R_{Ef} are the correlation coefficients of the best fit for $E_g(Y)$ and $E_F^{RT}(Y)$, respectively.

In a-Si:H films, there is a correlation known as the Meyer-Neldel rule between the pre-exponential factor, σ_0, and the activation energy, E_a [48]. Fig. 12(a) shows all the experimental points for our Si-Ge films deposited with different dilution in the coordinates σ_0 *vs.* E_a. The plot indicates a general trend of σ_0 increasing with E_a rather than a clear correlation. The correlation is strongest for the samples deposited with hydrogen dilution, re-plotted in Fig. 12(b). For this case, the correlation coefficient R = 0.95 and we can write:

$$\sigma_0 = \sigma_{00} \exp(E_a/E_0) \quad \text{…….. (11)}$$

where, σ_{00} = 5.75 $Ohm^{-1}cm^{-1}$ and E_0 = 0.1eV. For comparison σ_{00} = 1 $Ohm^{-1}cm^{-1}$ and E_0 = 0.064 eV for amorphous silicon [48]. The M-N model with σ_{00} = 1 $Ohm^{-1}cm^{-1}$ E_0 = 0.067 eV

has been reported by Y. Yukimoto [49] for Si-Ge films deposited by RF discharge using a feed gas of SiH_4, GeH_4, H_2 and He. It should be noted that the M-N models for a-SiH films are still debated [49-51] and poorly understood for binary alloys. In fact, there is not enough experimental data for proper discussion of the models.

The last quantity, to be extracted from the temperature dependence of the conductivity, is the γ-factor. Fig. 13 shows the γ-factor points plotted *vs.* the Ge content in the various films. The points demonstrate significant scattering rather than a clear correlation. Nevertheless, there is some indication of a change in sign of the γ-factor in the films at high Ge content. For H-dilution and without dilution, the change in sign occurs at $Y \approx 0.8$ and for Ar dilution at $Y \approx 0.95$. This corresponds to Fermi levels $E_F \approx 0.33$eV and $E_F \approx 0.25$ eV, respectively, which suggests local minima of density of states in the vicinity of these energies. This position of local minimum agrees with the density of state model reported by Stutzman et al.[42, Fig.26].

4. Discussion

The growth of any film by PE CVD is a complex process. Even for pure silicon films the understanding is incomplete let alone for two component compositions such as silicon-germanium. In general, it is possible to divide the process into several categories. a) Gas phase processes and bulk plasma processes that determine the gas composition including neutrals (radicals, atoms, and molecules), ions and electrons. For film growth, active radicals are of great importance. b) In plasmas with capacitance excitation there are sheath regions

with properties different from the bulk plasma. The growing surface is in contact with the sheath region resulting in ion bombardment of the surface. For alternating current discharges, electrons bombard the growing surface during part of the cycle. c) Gas-solid processes occur on the surface of the growing film. Important steps include creation of sites for growth, sticking and desorption, surface diffusion, and surface chemical reactions such as hydrogen extraction. The effect of ion bombardment is significant and depends on chemical reactivity and mass of the ions, sheath potential, pressure, and discharge frequency [52-54]. The effect of ion bombardment has not been well studied. Nevertheless Dalal *et al.* [55] have reported a positive effect of ion bombardment for deposition of Si-Ge films by ECR discharge. An increase of growth rate with Ge in the gas feed was observed by Yu-Pin Chou and Si-Chen Lee [56]. They observed that the growth rate showed a nearly monotonic increase as X increased from 0 to 0.8, followed by reduction as X increased from 0.8 to 1.

We observed a monotonic increase of the deposition rate over the entire range of X for the films deposited with or without H-dilution. The films deposited with Ar-dilution showed a reducing deposition rate in the range X from 0.1 to 0.2 and an increasing rate in the range from X = 0.2 to 1.0. For the films deposited without dilution this growth, $V_d(X)$, was practically linear, while for H-dilution a trend for V_d to saturate at $X > 0.5$ was observed. The increase of V_d with X has also been reported in refs. [38, 42]. In ref. [56], the authors attempted to explain this trend by the assumed difference in binding energies of Ge-H and Si-H. If the former is less than the latter, decomposition of GeH_4 will be faster, resulting in a higher concentration of Ge radicals, which will then become the more dominating pre-cursors. However, there is little difference in binding energy calculated from the enthalpy of the hydrogen bonds: 321.7 kJ/mol for Ge-H (E_b= 3.34 eV/bond) and 299.2 kJ/mol for Si-H

(E_b= 3.1 eV/bond) [58]. The cross-sections for SiH_4 and GeH_4 are also not expected to strongly differ since the atom radii are similar: $R_{Si} = 1.25x10^{-10}$m and $R_{Ge} = 1.11x10^{-10}$m [57]. For electron impact decomposition, the electron velocity in the molecule is important, but this also is practically the same for SiH_4 and GeH_4 molecules.

The arguments above suggest that the reason for the deposition rate increase with X might be related to processes on the surface of the growing film, including ion bombardment. For these processes, the difference in Si and Ge masses (m_{Si} = 28 a.u., m_{Ge} = 73 a.u.) is of great importance. The effect of ion bombardment for the different types of dilution (m_{Ar} = 40 a.u. and m_H = 1 a.u.) is also expected in this case. The two main processes that occur on the growing surface are sticking of the precursors to the film and surface diffusion of the adsorbed species (radicals). The latter is important for structure and properties of the film, while the former significantly influences the film growth rate. Sticking of each type of species (radicals) is characterized by the coefficient $s = N_s/N_{tot}$, where N_s is the number of molecules stuck to the surface and N is the total number of molecules that arrived. Conventionally, the SiH_3 radical is considered to be important for the growth of a-SiH films [58], while for Si-Ge growth a similar principal radical (or radicals) has not been revealed. For relatively low Ge concentrations, it is reasonable to consider incorporation of Si atoms in the lattice in a way similar to amorphous silicon film, but not for incorporation of Ge atoms. The rise in deposition rate with X should be related to Ge atoms and presumably with the sticking of Ge radicals (atoms). In this case the following questions should be answered: Why is s for Ge-radicals larger than that for Si-radicals? Why does dilution by H and by Ar affect the deposition rate?

The dependence of Ge content in the film on the Ge concentration in the feed mixture shown in Fig. 3 a) indicates clearly preferential incorporation of Ge atoms. Let us introduce the Ge-preference coefficient, P_{Ge}, as

$$P_{Ge} = [Y/(1-Y)]/[(X/(1-X)] \quad \ldots\ldots\ldots\ldots\ldots\ldots\ldots\ldots\ldots\ldots \quad (12)$$

From the best fit of the experimental data as shown for example in Fig. 3 b) to the theoretical curve (12), we obtain the single parameter of the fit, P_{Ge}. The result is $P_{Ge.} = 6.44 \pm 0.03$ (R= 1) for H-dilution, $P_{Ge} = 4.3 \pm 0.6$ (R=0.97) for Ar dilution, and $P_{Ge} = 3.9 \pm 0.2$ (R=0.98) for the films deposited without dilution. Preferential incorporation of Ge has been reported for RF discharge and silane+germane feed gases by Stutzman *et al.* [42] $P_{Ge} = 6 \pm 1$, and by Yu-Pin Chou [56] $P_{Ge} = 12$. The latter value reported is remarkably higher than those observed in this work, which could be related to differences in deposition conditions, including discharge frequency, geometry, gas flow, and substrate temperatures. It is interesting that the order of the values P_{Ge} correlates in inverse fashion with the order of the mass of the dominating species. Indeed, we can arrange P_{Ge} from maximum to minimum value as: P_{Ge}= 6.44, 4.3 and 3.9 for the films deposited with H-, Ar- and without dilution, respectively. The corresponding mass of the dominating species is, of course, M_H=1, M_{Ar}=40 and M_{Ge}=72. During film deposition there is a sheath potential U_{sheath} between the growing surface and the bulk plasma. This potential accelerates ions moving from the plasma bulk to the growing surface resulting in ion bombardment with ion energy $E_i \approx eU_{sheath}$. The effect of the ion bombardment depends on both E_i and the energy transfer efficiency from the ion to the lattice. The efficiency is highest, when the ion mass is equal to that of the lattice atom, while

light ions are reflected almost elastically, without energy transfer. This suggests that ion bombardment is a significant factor in Ge incorporation.

Another kind of preference that should be discussed is related to hydrogen bonding in the films. In a-SiH films, it is well known that the material should have an optimal concentration of hydrogen and optimal microstructure, e.g. no $Si-H_2$ bonding, to minimize the concentration of dangling bonds. For the case of Si-Ge films, there is insufficient knowledge and understanding of these problems. What is the optimal hydrogen concentration? How should hydrogen be distributed between Si and Ge atoms? What is the optimal microstructure for both Si-H and Ge-H bonding for achieving good electronic properties? To the knowledge of the authors, there is very limited information about these questions for films deposited by the commonly used methods of RF discharge [42] and ECR discharge [43]. There are no reports on these questions for the films deposited by LF discharge. It should be noted that it is not sufficient just to demonstrate IR spectra indicating significant Ge-H absorption; the latter must be compared with that for Si-H bonds. Our data in Table 2 has revealed the effect of gas dilution on the preference factor of Ge-H bond formation $P_{Ge-H,}$ please see section 3.6.1. It should be noted that we observed $P_{Ge-H} < 1$ in all the samples independent of dilution. This means that germanium atoms are terminated with hydrogen less frequently than silicon atoms. The minimum $P_{Ge-H} = 0.29$ value was observed for the films deposited without dilution and the maximum value, $P_{Ge-H}=0.61$, was observed for the films deposited with Ar dilution.

It is interesting to compare the hydrogen distribution between Si and Ge atoms and the incorporation of Ge atoms. From this comparison we can see that we have: 1. High Ge

preference and low Ge-H preference in the films with H-dilution, 2. Moderate Ge preference and higher Ge-H preference in the films deposited with Ar dilution, 3. Low Ge preference together with very low Ge-H preference in the films deposited without dilution. In other words, in the case of H-dilution, the films grow with strong preference for Ge incorporation, but these Ge atoms can create dangling bonds, because of less frequent termination with hydrogen. When Ar dilution is used, Ge preference is less and Ge-H preference is higher. Finally, for deposition without dilution we observe the lowest Ge preference and the lowest Ge-H preference, which means that in this case, Ge atoms are incorporated more readily with respect to their proportion in the feed gas, but their hydrogen termination is worse. Two other important results from our IR spectra are the dependence of hydrogen and oxygen content in our films upon Ge content. In all the films studied, we observed reducing hydrogen content with Y (Fig.6). The effect of dilution on this trend was not strong. Reduction of hydrogen with Y has been reported previously [59], but without explanation or proposed mechanism. Oxygen content determined by both SIMS and IR was also found to decrease with Y (Fig.7). This trend has been published previously [40] but again without explanation or mechanism for this behavior.

Let us start by considering the dependence of the optical properties and the optical gap upon Ge content in the films. A linear dependence of the optical gap on the Ge content has been reported for LF discharge: E_g=1.71- X for X=0 –0.5 [61]; for RF discharge: E_{04} =1.92-0.79Y, Y = 0-1.0 [38]; and for anodic films [18], E_g=1.76-0.78Y [61] E_g= 1.73- 0.71Y [62]. In our work, the dependence of the optical gap on Ge content can be fitted by E_g=1.7-0.7Y, which is in reasonable agreement with the previously reported expressions. The value of ΔE that

characterizes the density of states of the band tails changed with Ge content and shows a maximum at Y ≈ 0.6 for the films deposited with H- or Ar dilution. This can presumably be related to the rise of structural disorder (composition fluctuations) for the films with approximately equal concentrations of Si and Ge atoms. Sheng *et al.* [63] have reported long-range fluctuations caused by compositional disorder for Y > 0.5. Additionally, there is evidence from AFM measurements that for such films some peculiarities of $L_c(Y)$ are observed as indicated in Table 1. The increase of the average grain diameter with Y for a-Si-Ge films deposited by LF discharge from 81.5 to 106 nm has been reported by Budaguan *et al.* [61]. The reasons for the ΔE minimum at Y = 0.45 for the films deposited without dilution is not clear at present, but could be caused by a reduction in tensile stress when Ge atoms are incorporated in an optimal concentration. Alternatively, processes on the growing surface could be responsible. In this case, however, one would expect some features on $V_d(Y)$, which have not been observed. Wickboldt *et al.* [18] found no correlation of ΔE to the optical gap in Si-Ge films deposited by RF plasma, but their experimental data exhibit significant scatter.

The absorption coefficient, α, measured at λ = 0.63 μm by both optical transmission T(λ) and variable angle ellipsometry, exhibits a linear dependence with Y as shown in Fig. 9. The values obtained by transmission measurements were systematically higher. This can be related to the fact that T(λ) measurements are sensitive to bulk properties, while VAE measurements are more sensitive to the sample surface which can contain an oxide layer or can otherwise differ from the bulk composition. The refractive index measured by VAE at λ = 0.63 μm changed abruptly from n = 3.91 (characteristic of a-Si film) to n = 5.4

(characteristic of a-Ge) even at low Y = 0.23. The index of refraction increased further to n = 5.99 at Y = 1.

All specimens exhibited an activation behavior for the temperature dependence of conductivity, $\sigma(T)$, as shown in Fig. 10. The conductivity was observed to increase with Ge content. Specifically, room temperature conductivity rises by about 7 orders of magnitude and the activation energy reduces, when Y changes from 0 to 1. It is interesting to compare the behavior of the Fermi level position, E_F, and the band gap, E_G, with Ge content as shown in Fig. 11. Here, the Fermi level behavior can be fit to a linear dependence: $E_F(Y)=0.72 - 0.50Y$. By comparing $E_F(Y)$ to $E_G(Y)$, it can be concluded that the Fermi level moves from approximately mid-gap for Y = 0 to the edge of the conduction band with increasing Y, *i.e.* the films become more n-type. However, P. Wickboldt *et al.* [18] reported no shift of E_F with Y for the films deposited by RF discharge. Non-linear behavior of the Fermi level position with Ge content has been reported in ref. [38]. The behavior of the conductivity pre-factor and γ-factor is discussed in Section 3.7.

5. Conclusions

Deposition processes, structure, and optical and electrical properties have been studied in $Si_{1-Y}Ge_Y$:H films deposited by LF PECVD over the entire range of compositions ($0 \le Y \le 1$) from SiH_4 and GeH_4 feed gas mixtures with and without dilution by hydrogen or by argon. From the observations and data analysis we can draw the following conclusions:

1) Dilution by hydrogen or by argon decreases the deposition rate. The deposition rate increases with Ge content.

4) Ge atoms are preferentially incorporated according to a preference factor, P_{Ge}, ranging from a maximum of 6.44 for deposition with hydrogen dilution to a minimum of 3.9 for the films deposited without dilution;

5) For all films, the hydrogen content decreases as Y increases. Similar behavior is observed for oxygen.

6) Hydrogen preferentially terminates at Si atoms. The preferential factor $P_{Ge\text{-}H} = 0.29$ for no dilution (the worst case) and $P_{Ge\text{-}H} = 0.61$ for argon dilution (the best case).

7) The optical gap decreases linearly with Ge content to as small as $E_g \approx 0.92\text{-}0.95$ eV at Y=1 (a-Ge);

8) The energy characterized band tail states ΔE achieves a maximum at $Y \approx 0.6$ in the films deposited with hydrogen or argon dilution and continuously increases with Y for the films deposited without dilution.

9) The optical constants measured by VAE (a surface sensitive technique) are in reasonable agreement with published data. The absorption coefficient and the refractive index obtained by VAE in comparison with data obtained from spectral transmission measurements (a bulk sensitive technique) suggest the films contain a surface layer with oxides and pores.

10) Ge content increases the conductivity of the films by about 7 orders of magnitude. Ge also reduces the activation energy for $\sigma(T)$. The effect of Ge on the temperature dependence depends on the amount and species of dilution.

11) The Fermi level position changes approximately linearly with Y. Comparing this behavior with that of the optical gap suggests the Fermi level shifts from about the middle of

the gap at low Y to the conduction band edge at high Y, *i.e.* the films become more n-type as Ge is incorporated.

12) The conductivity pre-exponential, σ_0, does not show a correlation with activation energy, *i.e.* there is no evidence for an analog to the Neyer-Mendel rule found for amorphous silicon;

13) The conductivity γ-factor changes sign at Y=0.8 for deposition with or without H-dilution and at Y=0.95 for Ar dilution. This suggests local minima in the density of states at $E \approx 0.33$eV and at $E \approx 0.25$ eV for the two cases.

Acknowledgement

The co-authors from INAOE acknowledge the support of this research by CONACyT project No. 42367 (CIAM-2002 Program). Work by TEF was performed under the auspices of the US Department of Energy by the University of California Lawrence Livermore National Laboratory under contract No. W-7405-Eng-48.

References:

1. J. K. Rath, F. D. Tichelaar, R. E. I. Schropp: Heterogeneous growth of microcrystalline silicon germanium. *Solar Energy Materials & Solar Cells* 74, 533 (2002).

2. M. Isomura, K. Nakahata, M. Shima, S. Taira, K. Wakisaka, M. Tanaka and S. Kiyama: Microcrystalline silicon–germanium solar cells for multi-junction structures. *Solar Energy Materials & Solar cells* **74**, 519 (2002).

3. M. Krause, H. Stiebig,. R. Carius, and H.Wagner: Microcrystalline germanium photodetectors , *Mat. Res. Soc. Symp. Proc.* **664**, A26.5 (2001).

4. G. Masini, V. Cencelli, L. Colace, F. DeNotaristefani and G. Assanto: A germanium photodetector array for the near infrared monolithically integrated with silicon CMOS readout electronics. *Physica E* **16**, 614 (2003).

5. R. Ambrosio, A. Torres, A. Kosarev, A. Heredia and M. Garcia: Amorphous $Si_{1-y}Ge_y$:H,F films obtained by low frequency PECVD for uncooled microbolometers. *Mat.Res. Soc. Symp. Proc.* **808,** A4.29 (2004).

6. A. Torres, A. Kosarev, M. L. Garcia and R. Ambrosio: Uncooled micro-bolometer based on amorphous germanium film. *J. Non-Cryst. Solids.* **329**, 179 (2003).

7. M. Garcia, R. Ambrosio, A. Torres and A. Kosarev: IR bolometers based on amorphous silicon germanium alloys. *J. Non-Cryst. Solids.* **338-340**, 744 (2004).

8. W. B Jordan., S.Wagner: Nanocrystalline Germanium p-i-n structures. Mat.Res. Soc. Symp. Proc., **808,** A 9.47 (2004).

9. Luft W., Y.Simon Tsuo: Hydrogenated amorphous silicon alloy deposition processes, (Marcel Dekker, Inc., 1993).

10. T. Searle: Properties of amorphous silicon and its alloys. EMIS Datareviews Series No.19, INSPEC 1998.

11. Y. Liu and V.L. Dalal: Properties of Amorphous Silicon-Germanium Films and Devices Deposited at Higher Growth Rates , *Mat. Res. Soc. Symp*. **715**, A18.3 (2002).

12. H. Matsumura, M.Yamaguchi, K.Morigaki: Properties of catalytic CVD amorphous silicon germanium (a-SiGe:H). Mat.Res.Symp.Proc. **192**, 499 (1990).

13. V. L. Dalal, Y. Liu, Z. Zhou and K. Han: Growth and properties of low bandgap amorphous (Si, Ge) alloy materials and devices**.** *J. Non-Cryst. Sol.* **299-302**, 1127 (2002) .

14. M. A. Lieberman and A. J. Lichtenberg: Principles of Plasma Discharges and Material Processing. (J. Wiley and Sons, NY, 1994) pp.333.

15. B. G. Budagian , A. A. Sherechenkov, G. L. Gorbulin and V. D. Chernomordic: Characterization of high rate a-SiGe:H thin films fabricated by 55 kHz PECVD. *Physica B* **325,** 394 (2003).

16. K. D. Mackenzie, J. R. Eggert, D. J. Leopold, Y. M. Li, S. Lin and W. Paul: Structural, electrical, and optical properties of a-$Si_{1-x}Ge_x$:H and an inferred electronic band structure. *Phys. Rev*. **B 31**, 2198 (1985).

17. Y. Liu and V. L. Dalal: Properties of Amorphous Silicon-Germanium Films and Devices Deposited at Higher Growth Rates. *Mat. Res. Soc. Symp.* **715**, A18.3 (2002).

18. P. Wickboldt, D. Pang, W. Paul, J. H. Chen, F. Zhong, C. C. Chen, J. D. Cohen, and L.Williamson: High performance glow discharge a-$Si_{1-x}Ge_x$:H of large x. *J. Appl. Phys.* **81**(9), 6252 (1997).

19. Y.S.Tsuo, Y.Xu, E.A.Ramsay, R.S.Crandall, S.J.Salamon, I.Balberg, B.P.Nelson, Y.Xiao, Y.Chen:Methods of improving glow-discharge-deposited a-SiGe:J. Mat.Res.Symp.Proc., **219**, 769 (1991).

20. M. Shima, A. Terakawa, M. Isomura, H. Haku, M. Tanaka, K. Wakisaka, S. Kiyama and S. Tsuda: Effects of very high hydrogen dilution at low temperature on hydrogenated amorphous silicon germanium. *J. Non-Cryst. Sol.* **227-230**, 442 (1998).

21. S.Miyazaki, H. Takahashi, H. Yamashita and M. Hirose: Growth and characterization of microcrystalline silicon–germanium films. *J. Non-Cryst. Sol*. **299-302**, 148 (2002).

22. M. E. Gueunier, J. P. Kleider, R. Bruggemann, S. Lebib, P. Roca I Cabarrocas, R. Meaudre and B. Canut: Properties of polymorphous silicon–germanium alloys deposited under high hydrogen dilution and at high pressure. *J. Appl. Phys.* **92(9)**, 4959 (2002).

23. W. B. Jordan S. Wagner: Effects of deposition temperature and film thickness on the structural, electrical, and optical properties of germanium thin films. *Mat. Res.Symp.Proc.* **715** , A18.2 (2002).

24. M. H. Brodsky, M. Cardona, and J. C. Cuomo: Infrared and Raman spectra of the silicon-hydrogen bonds in amorphous silicon prepared by glow discharge and sputtering. *Phys. Rev.* **B 16,** 3556 (1977).

25. R. Swanepoel: Determination of the thickness and optical constants of amorphous silicon. *J. Phys. E*: *Sci. Instrum.* **16**, 1214 (1983).

26. R.Swanepoel: Determination of surface roughness and optical constants of inhomogeneous amorphous silicon films. *J. Phys. E*: Sci. Instrum. **17**, 896 (1984).

27. Y. Zhao, Gwo-Ching Wang, Tong-Ming Lu: Characterization of amorphous and crystalline rough surface: principles and applications, (Academic Press, 2001) p.7-16.

28. D. Comedi, F. Dondeo, I. Chambouleyron, Z. L. Peng and P.Masher: Compact hydrogenated amorphous germanium films by ion-beam sputtering deposition. *J. Non-Cryst. Sol.* **266-269**, 713 (2000).

29. G. Lukovsky, S. S. Chao, J. Yang, J. E. Tyler, R. C. Ross and W.Czubatyj: Chemical bonding of hydrogen and oxygen in glow-discharge–deposited thin films of a-Ge:H and a-Ge:(H,O). *Phys. Rev.* **B 31**, 2190 (1985).

30. M. N. Makadzi, M. F. A. Alias, A. A. Essa, H. R. Al-Azawi: FT-IR and XPS analysis of a-Si1-xGex:H thin films. *Renewable Energy* **28**, 975 (2003).

31. G. Lukovsky, J. Yang, S. S. Chao, J. E. Tyler and W. Chubatyj: IR absorption in glow-discharge-deposited a-Si:(D,O) and a-Si:(D,N) alloy films. *Phys. Rev.* **B 29**, 2302 (1984).

32. G.Lukovsky and J. D. Joannopoulos: The physics of Hydrogenated Amorphous Silicon. (VII, Springer, Berlin, 1984) p.235

33. C. J. Fang, R. J. Gruntz, L. Ley, M. Cardona, F. J. Demond, G. Muller and S. Kalbitzer: The hydrogen content of a-Ge:H and a-Si:H as determined by ir spectroscopy, gas evolution and nuclear reaction techniques. *J. Non-Cryst. Sol.* **35-36**, 255 (1980).

34. W. Beyer: Diffusion and Solubility of Hydrogen in Amorphous and Microcrystalline Si:H Films. *Mat. Res. Soc. Symp. Proc.* **664**, A13.1 (2001).

35. W.A.Lanford, H.P.Trautvetter, J.F.Ziegler and J.Keller: New precision technique for measuring the concentration versus depth of hydrogen in solids. *Appl. Phys. Lett.* **28**(9), 566 (1976).

36. R. C. Ross, I. S. T. Tsongm, R. Messier, W. A. Lanford and C.Burman: Quantification of hydrogen in a-Si:H films by ir spectrometry, N nuclear reaction, and SIMS. *J. Vac .Sci. Technol*. **20**, 406 (1982).

37. M.Cardona: Vibrational-spectra of hydrogen in silicon and germanium. *Physica Status Solidi b* 118, 463 (1983).

38. K. D. Mackenzie, J. R. Eggert, D. J. Leopold, Y. M. Li, S. Lin and W. Paul: Structural, electrical, and optical properties of a-$Si_{1-x}Ge_x$:H and an inferred electronic band structure. *Phys. Rev*. **B 31**, 2198 (1985).

39. A. A. Langford, M. L. Fleet, B. P. Nelson and N. Maley: Infrared Absorption Strength and Hydrogen Content of Hydrogenated Amorphous Silicon, *Phys. Rev.* **B 45**, 13367 (1992).

40. B. P. Nelson, Y. Xu, J. D. Webb, A. Mason, R. C. Reedy, L. M. Gedvilas and W. A. Lanford: Techniques for measuring the composition of hydrogenated amorphous silicon–germanium alloys. *J. Non-Cryst. Sol.* **266-269**, 680 (2000).

41. W. Paul, D. K. Paul, B. Von Roedern, J. Blake and S. Oguz: Preferential Attachment of H in Amorphous Hydrogenated Binary Semiconductors and Consequent Inferior Reduction of Pseudogap State Density. *Phys. Rev. Lett.* **46**, 1016 (1981).

42. M. Stutzmann, R. A. Street, C. C. Tsai, J. B. Boyce and S.E.Ready: Structural, optical, and spin properties of hydrogenated amorphous silicon-germanium alloys. *J. Appl. Phys*. **66**, 569 (1989).

43. V.L.Dalal: Growth chemistry of amorphous silicon and amorphous silicon-germanium alloys. Current opinion in Solid State&Material Science, **6**, 455 (2002).

44. N.F.Mott, E.A.Davis: Electronic Processes in Non-Crystalline Materials. (Clarendon press, Oxford, 1979).

45. Handbook of Optical constants of Solids II, (Ed. by Edward Palik, Academic Press Inc.) p.774

46. R. F. Potter: Optical constants of germanium in spectral region from 0.5 to 3.0 eV. *Phys.Rev* **150**, 562 (1966).

47. P. Nagels, in *Amorphous Silicon,* edited by M. H. Brodsky, (Springer, NY, 1979) p.122.

48. D. E. Carlson, C. R. Wronski. in *Amorphous semiconductors*, edited by M. H. Brodsky, (Springer NY, 1979) p.299.

49. Y. Yukimoto in JARECT v.6 *Amorphous Semiconductor Technologies and devices*, edited by Y. Hamakawa, (1983) p.136.

50. W. B. Jackson: Connection between the Meyer-Neldel relation and multiple-trapping transport. Phys. Rev. **B 38**, 3595 (1988).

51. M.Kikuchi: The Meyer–Neldel rule and the statistical shift of the Fermi level in amorphous semiconductors. *J. Appl. Phys.* **64**, 4997 (1988).

52. P. Roca I Canbarrocas, P. Morrin, V. Chu, J. P. Conde, J. Z. Liu, H. R. Park and S. Wagner: Optoelectronic properties of hydrogenated amorphous silicon films deposited under negative substrate bias. *J. Appl. Phys*. **69**, 2942 (1991).

53. B. Kalache, A. I. Kosarev, R.Vanderhagen, P. Roca I Cabarrocas: Ion bombardment effects on microcrystalline silicon growth mechanisms and on the film properties. *J. Appl. Phys*. **93** (2), 1262 (2003).

54. E.A.G.Hammers, A.Fontcuberta, I Morral, C.Niikura, R. Brenot and P. Roca I Cabarrocas: Contribution of ions to the growth of amorphous, polymorphous, and microcrystalline silicon thin films. *J. Appl. Phys*. **88**, 3674 (2000).

55. V.L.Dalal, S.Haroon, Z.Zhou, T.Maxson and K.Han: Influence of plasma chemistry on the properties of a-(Si,Ge):H alloys. *J. Non-Cryst So.l* **266,** 675 (2000).

56. Yu-Pin Chou and Si-Chen Lee: Structural, optical, and electrical properties of hydrogenated amorphous silicon germanium alloys. *J. Appl. Phys.* **83**, 4111 (1998).

57. www.webelements.com

58. A. Matsuda: Plasma and surface reactions for obtaining low defect density amorphous silicon at high growth rates. *J. Vac. Sci.Technol. A* **16**, 365 (1998).

59. Y T.Simizu, M.Kumeda, A.Morimoto, Y.Tsujimura, I.Kobayashi.\: NMR and ESR studies on a-SiGe:H films prepared by glow discharge and magnetron sputtering. Mat.Res. Symp. Proc., **70,** 313 (1986).

60. B. G. Budaguan, A. A.Sherchenkov and G. L. Gorbulin: The properties of a-SiGe:H films deposited by 55 kHz PECVD. *J. Non-Cryst. Sol.* **297**, 205 (2002).

61. K. D. Mackenzie, J. H. Burnett, J. R. Eggert, Y. M. Li and W. Paul: Comparison of the structural, electrical, and optical properties of amorphous silicon-germanium alloys produced from hydrides and fluorides. *Phys. Rev.* **B38**, 6120 (1988).

62. K. D. Mackenzi, J. Hanma, J. R. Eggert, Y. M. Li, Z. L. Sun and W.Paul: Properties of a-$Si_{1-x}Ge_x$:H and a-$Si_{1-x}Ge_x$:H:F alloys. *J. Non-Cryst. Sol.* **77-78**, 881 (1985).

63. S. R. Sheng, M. Boshta, R. Braunstein and V. Dalal: On the electronic transport properties of amorphous (Si,Ge) alloys: charged scattering centers and compositional disorder. *J. Non-Cryst. Sol.* **303**, 201 (2002).

List of tables:

Figure Legends

Fig.1. Deposition rate as a function of X, the germane content in the feed gas, X, defined as the gas flow ratio $X=Q_{GeH4}/Q_{SiH4+GeH4}$.

Fig.2. SIMS profiles for $Si_{1-Y}Ge_Y$:H films deposited with H-dilution and various values of the germane content in the feed gas, X=0.1 (a), 0.5 (b) and 1(c).

Fig.3. Germanium (Ge) content in film, Y, versus germane (GeH_4) content in feed gas, X (a), and an example of Y(X) best fit to eq.(12) with P_{Ge} as variable parameter for the films deposited with H-dilution.

Fig.4. General view of IR spectra of the $Si_{1-Y}Ge_Y$:H samples deposited with different dilutions and X=0.1(a) and X=1(b). The IR spectrum for a-Si:H film (X=0) is shown for comparison.

Fig.5. Dependence of hydrogen content, C_H, in the film on Ge-content, Y, determined from both FTIR and SIMS data.

Fig.6. Oxygen content determined by both SIMS and FTIR as a function of Ge- content in solid phase $C_O(Y)$ for $Si_{1-Y}Ge_Y$:H films deposited with different dilutions.

Fig.7. Spectral dependence of optical absorption coefficient: $\alpha(h\nu)$ (a) and Tauc plots $\sqrt{\alpha h\nu}=f(h\nu)$ (b) of the $Si_{1-Y}Ge_Y$:H films deposited from the gas mixtures with different Ge-content Y and different dilutions.

Fig.8. Band tail characteristic energy as a function of Ge content, ΔE (Y). The solid lines are shown as guide to the eye.

Fig.9. Absorption coefficient at $\lambda = 0.63$ μm as a function of Ge content in the film $\alpha_{0.6}=f(Y)$, determined from measurement of transmission and VAE .

Fig.10. Temperature dependence of conductivity $\sigma(T)$ for the Si-Ge films deposited with various Ge content, Y, and dilutions.

Fig.11. Fermi level position, E_F, and optical gap, E_g, *vs.* Ge content in film, Y.

Fig.12. Pre-exponential factor σ_0 *vs.* E_a: for all samples (a) and for samples deposited with H-dilution (b).

Fig.13. γ-factor for the temperature dependence of conductivity as a function of Ge content (Y) for all samples.

Table 1. Surface morphology parameters obtained from AFM measurements

Sample #	X	Y	Dilution	Morphology parameters			
				Ave. Height, <Z>, nm	R_a nm	RMS R_q, nm	Correlation length, L_c nm
170	0	0	H_2	5.1	0.79	1.0	60
171	0.1	0.42	H_2	7.6	0.6	0.8	17
173		0.23	Argon	6.3	1.7	2.3	72
175		0.33	None	3.1	0.6	0.8	42
181	0.2	0.62	H_2	9.4	1.6	2.1	95
183		0.60	Argon	6.7	1.6	2.0	40
186		0.45	None	8.5	2.1	3.0	58
188	0.5	0.87	H_2	12.3	3.1	4.0	55
190		0.90	Argon	9.0	1.3	1.8	85
192		0.79	None	35	13	15	149

Table 2. FTIR data for the $Si_{1-Y}Ge_Y$:H films

Sample	*K* [cm^{-1}]	*W* [cm^{-1}]	*S* [cm^{-2}]	Bonding
S170 a-Si:H X=0 Y=0	644.5 ± 0.4	78.2 ± 0.7	(8.76 ± 0.07) E4	SiH_n
	999 ± 3 1051.5± 0.7	104± 2 60 ± 3	(9.4 ± 0.5) E4 (3.2 ± 0.5) E4	Si-O in different configurations
	2004.3± 0.9 2079.4± 0.8	71.8 ± 0.8 88.5 ± 0.8	(1.38± 0.05) E4 (2.73 ± 0.05) E4	SiH SiH or SiH_2
S171 X=0.10 Y=0.42 H-dilution`	550 ± 20 592± 3 647 ± 5	52 ± 7 58 ± 10 62 ± 3	(1.7 ± 1.7) E4 (7 ± 3) E4 (6 ± 1) E4	GeH_n GeH_n SiH_n
	782.4 ± 0.8 872 ± 6 966 ± 3 1058± 3	46 ± 1 79 ± 7 104 ± 7 43 ± 9	(6.8 ± 0.3) E3 (1.3 ± 0.4) E4 (5.0 ± 0.4) E4 (1.5 ± 0.8) E36	GeH_n(?), Si-O-Si-H_n(?) Ge-O-Ge GeO, Si-O, (?) Si-O
	1885.4± 0.5 2025.8± 0.3	66 ± 1 95.0 ± 0.7	(1.45± 0.02) E4 (4.30 ± 0.02) E4	GeH SiH
S174 with Si_3N_4 X=0.10 Y=0.23 Ar dilution	596 ± 2 653 ± 2	71 ± 1 60 ± 1	(5.3 ± 0.2) E4 (2.8 ± 0.2) E4	GeH_n SiH_n
	798 ± 3 874 ± 2 968 ± 2	58 ± 4 77 ± 6 122.4 ± 2.	(6.0 ± 0.8) E3 (1.4 ± 0.2) E4 (5.2 ± 0.2) E4	GeH_n(?) Si-CH_3(?) Ge-O-Ge Si-O(?), Ge-O(?)
	1883.9± 0.8 2031.8± 0.4	61 ± 2 112.7 ± 0.8	(5.0 ± 0.1) E3 (2.79 ± 0.02) E4	GeH SiH
S175 X=0.10 Y=0.33 No dilution	619.9 ± 0.2	104 ± 1	(1.49 ± 0.02) E5	SiH_n
	881.3 ± 0.6 964.6 ± 0.3	32 ± 1 101.0 ± 0.6	(2.0 ± 0.1) E3 (3.44 ± 0.02) E4	Ge-O-Ge Si-O? Ge-O(?)
	1883 ± 1 2030.2± 0.3	59 ± 2 109.7 ± 0.8	(6.9 ± 0.2) E3 (4.84 ± 0.03) E4	GeH SiH
S181 X=0.20 Y=0.62 H-dilution	584.7 ± 0.7 652 ± 1	78.9 ± 0.8 54.0 ± 1	(7.5 ± 0.1) E4 (1.7 ± 0.1) E4	GeH_n SiH_n
	875 ± 1 953.1±7.21 1025.4±32.2	43 ± 4 103.4 ± 7.3 89 ± 20	(2.0 ± 0.4) E3 (2.7 ± 0.4) E4 (3 ± 4) E3	Ge-O-Ge Si-O? Ge-O(?) Si-O
	1881.9 ± 0.2 2016.8 ± 0.3	65.7 ± 0.4 82.5 ± 0.6	(2.13 ± 0.01) E4 (2.32 ± 0.01) E4	GeH SiH
S183 X=0.20	586.6 ± 0.9 652 ± 1	75 ± 1 57 ± 1	(9.3 ± 0.2) E4 (3.2 ± 0.2) E4	GeH_n SiH

Y=0.64 Ar dilution	766 ± 1 801 ± 2 867 ± 2 958 ± 1 1072.9 ± 0.7	25 ± 3 45 ± 7 60 ± 4 129± 2 28 ± 2	(1.1 ± 0.4) E3 (3.4 ± 0.7) E3 (6.1 ± 0.8) E3 (3.90 ± 0.08) E4 (9 ± 1) E2	GeH_n? GeH_n? $Si-CH_3$? Ge-O-Ge Si-O? Ge-O(?) Si-O
	1884.8 ± 0.3 2019.5 ± 0.3	65.5 ± 0.7 85.8 ± 0.7	(1.71 ± 0.01) E4 (2.67 ± 0.01) E4	GeH_n SiH_n
S186 X=0.20 Y=0.45 No dilution	593 ± 1 655 ± 1	73 ± 1 57 ± 1	(6.9 ± 0.2) E4 (3.2 ± 0.2) E4	SiH_2 Si-H
	878.9 ± 0.7 963.1 ± 0.3 1073± 1	38 ± 2 110 ± 1 25 ± 3	(1.8 ± 0.2) E3 (3.94 ± 0.03) E4 (5.6 ± 0.7) E2	Ge-O-Ge Si-O? Ge-O(?) Si-O
	1886.0± 0.6 2025.3± 0.3	64 ± 1 96.8 ± 0.7	(9.6 ± 0.1) E3 (2.98 ± 0.02) E4	GeH SiH
S188 X=0.50 Y=0.87 H-dilution	564 ± 3 620± 20	60 ± 3 83 ± 14	(3.4 ± 0.8) E4 (2.0 ± 0.8) E4	GeH SiH
	882 ± 4 977 ± 2 1060± 2	65 ± 8 110±20 49 ± 14	(7.3 ± 3.4) E3 (3.2 ± 0.6) E4 (2.9 ± 2.6) E3	Ge-O-Ge Ge-O(?) Si-O
	1874.1± 0.2 1998± 1	62.9 ± 0.3 93 ± 3	(2.49 ± 0.01) E4 (5.6 ± 0.1) E3	GeH SiH
S190 X=0.50 Y=0.90 Ar dilution	560 ± 3 610± 11	65 ± 3 82 ± 7	(5 ± 1) E4 (4 ± 1) E4	GeH SiH
	779 ± 1 912 ± 9 1014 ± 6	43 ± 4 160±11 106±14	(1.7 ± 0.3) E3 (4.4 ± 0.5) E4 (7.3 ± 4.6) E3	(?) Ge-O(?) Si-O
	1878.4± 0.2 2010.6± 0.7	59.9 ± 0.3 66 ± 1	(2.54 ± 0.01) E4 (6.9 ± 0.1) E3	GeH_n SiH_n
S192 X=0.50 Y=0.79 No dilution	562 ± 3 617 ± 8	66 ± 2 81 ± 6	(3.7 ± 0.7) E4 (3.3 ± 0.7) E4	GeH SiH
	883 ± 3 961 ± 2 1045.2 ± 0.7	71± 2 95 ± 4 41 ± 2	(4.8 ± 0.8) E3 (1.93 ± 0.09) E4 (1.2 ± 0.2) E3	Ge-O-Ge Ge-O(?) Si-O
	1875.7 ± 0.1 2013.8 ± 0.3	60.4 ± 0.2 67.6 ± 0.7	(2.253±0.007) E4 (8.7 ± 0.08) E3	GeH SiH
S195 with Si_3N_4 X=1.00 Y=1.00 H-dilution	556 ± 3 612 ± 4 684 ± 7	73 ± 3 57 ± 8 77± 9	(3.9 ± 0.3) E4 (1.1 ± 0.5) E4 (9 ± 2) E3	GeH SiH(?) SiH(?)
	897 ± 2 986 ± 1	120 ± 3 58 ± 3	(1.74 ± 0.04) E4 (4.0 ± 0.4) E3	Ge-O-Ge Ge-O(?)
	1873.5 ± 0.3	46.3 ± 0.6	(1.19 ± 0.01) E4	GeH

S197 with Si_3N_4 X=1.00 Y=1.00 Ar dilution	562 ± 1 630 ± 18	75 ± 3 120 ± 17	(3.7 ± 0.5) E4 (1.9 ± 0.5) E4	GeH SiH (?)
	887 ± 3 977 ± 2	106 ± 4 78 ± 2	(1.26 ± 0.06) E4 (7.5 ± 0.6) E3	Ge-O-Ge Si-O? Ge-O(?)
	1877.1 ± 0.4	51 ± 0.7	(1.58 ± 0.02) E4	GeH_n
S199 with Si_3N_4 X=1.00 Y=1.00 No dilution	557 ± 3 609 ± 6	67 ± 2 61 ± 4	(2.5 ± 0.3) E4 (10 ± 3) E3	GeH SiH(?)
	824 ± 1 887 ± 12	73 ± 4 120 ± 10	(1.7 ± 0.4) E4 (2.0 ± 0.4) E4	GeH_2, Ge-O-Ge
	1875.8 ± 0.4	49.4 ± 0.8	(1.48 ± 0.02) E4	GeH_n

Table 3. Optical characteristics: E_G , B, E_{03}, E_{04} for the $Si_{1-Y}Ge_Y$:H films.

Sample #	X	Y	Dilution	E_G (eV)	B $(eV.cm)^{-1/2}$	E_{03} (eV)	E_{04} (eV)	ΔE (eV)
128	0	0	Hydrogen	1.81	619 ± 12	1.86	2.04	0.18
172	0.10	0.42	Hydrogen	1.33	539 ± 74	1.37	1.55	0.18
174		0.23	Argon	1.39	485 ± 2	1.40	1.64	0.24
176		0.33	None	1.36	529 ± 3	1.41	1.58	0.17
182	0.20	0.62	Hydrogen	1.23	1101 ± 158	1.12	1.34	0.22
184		0.60	Argon	1.42	1229 ±163	1.20	1.48	0.28
187		0.45	None	1.44	1460 ± 258	1.37	1.52	0.15
189	0.50	0.87	Hydrogen	1.03	696 ± 48	1.01	1.20	0.19
191		0.90	Argon	1.17	1347 ± 172	0.98	1.22	0.23
193		0.79	None	1.05	483 ± 89	1.04	1.25	0.21
195	1.00	1.00	Hydrogen	0.99	563 ± 82	0.95	1.14	0.19
197		1.00	Argon	1.03	684 ± 153	0.96	1.17	0.21
199		1.00	None	0.98	650 ± 31	0.92	1.15	0.23

Note: error of E_G is less than 0.05 eV, error of the values E_{03}, E_{04}, and ΔE is less than 0.02 eV.

Table 4. Optical constants n, k, α measured by VAE for the $Si_{1-Y}Ge_Y$:H films[1]

X	Y	Dilution	Refractive index, n	Error σ_n	Extinctión coefficient k	Error σ_k	Thickness, d (Å)	Error σ_d (Å)	Absorption coefficient α (cm^{-1})
0	0	Hydrogen	3.9172	0.0003	0.0188	0.0002	9913.7	0.8	$3.7 \cdot 10^3$
0.1	0.42	Hydrogen	5.435	0.003	0.083	0.005	7003	4	$1.6 \cdot 10^4$
	0.23	Argon	5.4714	0.0004	0.01139	–	10501	3	$2.2 \cdot 10^3$
	0.33	None	5.46	0.01	0.07	0.01	10539	37	$1.4 \cdot 10^4$
0.2	0.62	Hydrogen	5.583	0.008	0.024	0.009	9706	15	$4.8 \cdot 10^3$
	0.60	Argon	5.64	0.02	0.08	0.01	8511	15	$1.6 \cdot 10^4$
	0.45	None	5.50358	0.03	0.045	0.004	10492	41	$9.0 \cdot 10^3$
0.5	0.87	Hydrogen	5.76	0.04	0.0028	0.0004	11563	13	$5.6 \cdot 10^2$
	0.90	Argon	5.660	0.006	0.035	0.006	8432	6	$7.0 \cdot 10^3$
	0.79	None	5.589	0.005	0.00308	–	11426	8	$6.1 \cdot 10^2$
1	1.00	Hydrogen	5.785	0.006	0.0203	0.002	10004	11	$4.0 \cdot 10^3$
	1.00	Argon	5.74	0.03	0.0124	0.001	10543	68	$2.5 \cdot 10^3$
	1.00	None	5.99	0.02	0.0097	0.001	13299	50	$2.0 \cdot 10^3$

[1] At wave lenght λ =0.6328 μm.

Table 5. Parameters obtained from temperature dependence of conductivity

Sample	x	Y	Dilution	σ_o [$\Omega^{-1}cm^{-1}$]	σ_{RT}, $Ohm^{-1}cm^{-1}$	E_a [eV]	$\gamma \times 10^4$ [eV/K]	E_F [eV]
170	0	0	Hydrogen	9	8E-10	0.60	2.67	0.52
172	0.10	0.42	Hydrogen	1400	8.6E-7	0.59	1.90	0.53
174		0.23	Argon	270	6.7E-8	0.62	0.52	0.61
176		0.33	None	240	1.1E-7	0.60	0.42	0.59
182	0.20	0.62	Hydrogen	850	3.3E-6	0.54	1.50	0.50
184		0.60	Argon	940	4.0E-7	0.60	1.60	0.55
187		0.45	None	1000	1.1E-7	0.64	1.60	0.59
189	0.50	0.87	Hydrogen	68	2.3E-3	0.29	-0.68	0.31
191		0.90	Argon	1400	3.0E-5	0.49	1.90	0.43
193		0.79	None	130	1.1E-5	0.46	-0.11	0.46
195	1.00	1.00	Hydrogen	92	4.3E-2	0.22	-0.41	0.23
197		1.00	Argon	110	6.3E-2	0.21	-0.27	0.22
199		1.00	None	280	1.45E-1	0.21	0.55	0.19

Note: error in determination of E_a and E_F is less than 0.05 eV

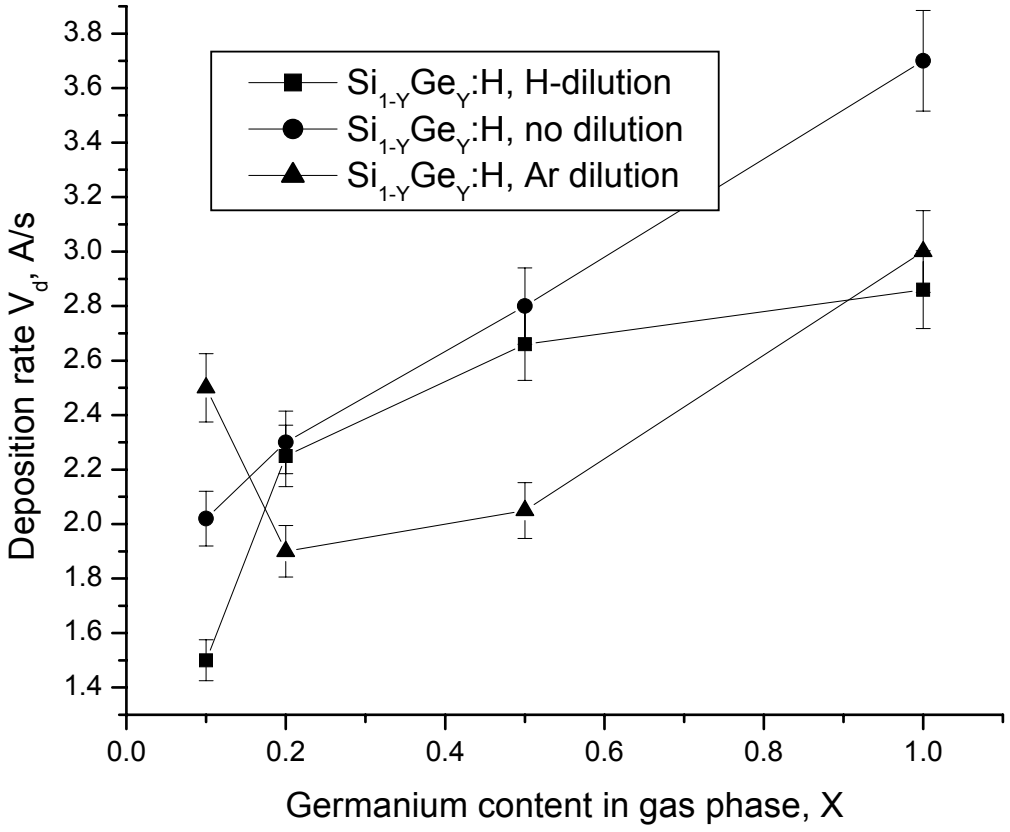
Si1-YGeY:H, H-dilution
Si1-YGeY:H, no dilution
Si1-YGeY:H, Ar dilution
Deposition rate Vd, A/s
Germanium content in gas phase, X
3.8
3.6
3.4
3.2
3.0
2.8
2.6
2.4
2.2
2.0
1.8
1.6
1.4
0.0
0.2
0.4
0.6
0.8
1.0

Fig. 1.

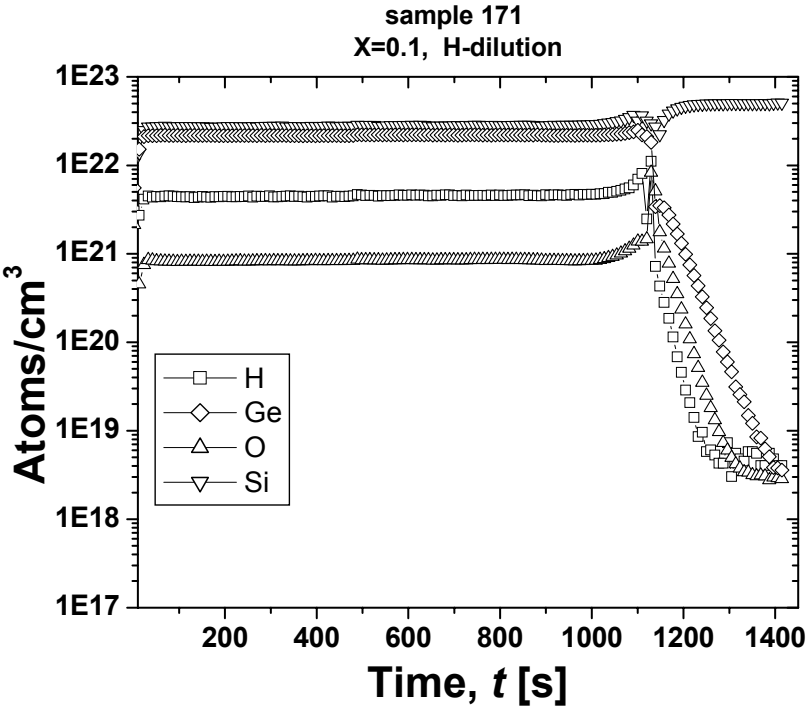
sample 171
X=0.1, H-dilution
Atoms/cm3
1E23
1E22
1E21
1E20
1E19
1E18
1E17
H
Ge
O
Si
200
400
600
800
1000
1200
1400
Time, t [s]

a)

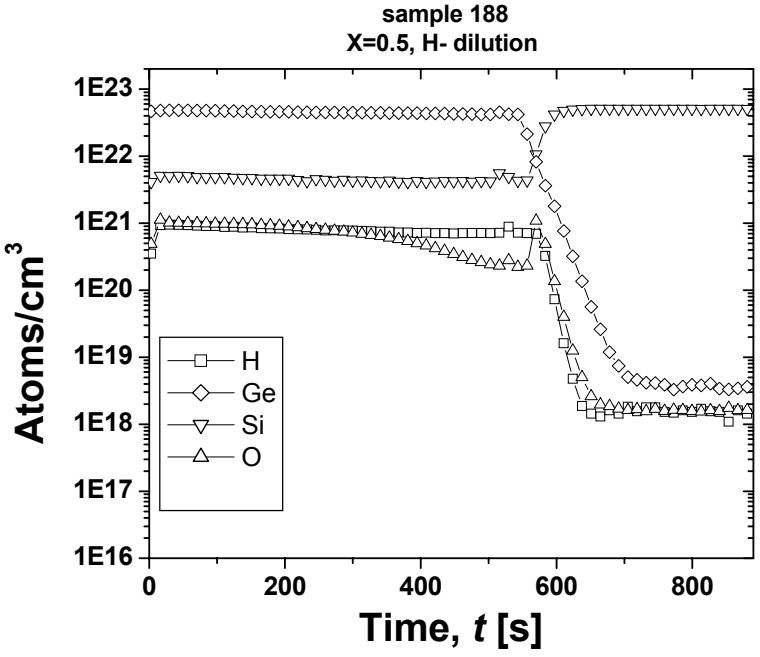
sample 188
X=0.5, H- dilution
Atoms/cm3
1E23
1E22
1E21
1E20
1E19
1E18
1E17
1E16
H
Ge
Si
O
0
200
400
600
800
Time, t [s]

b)

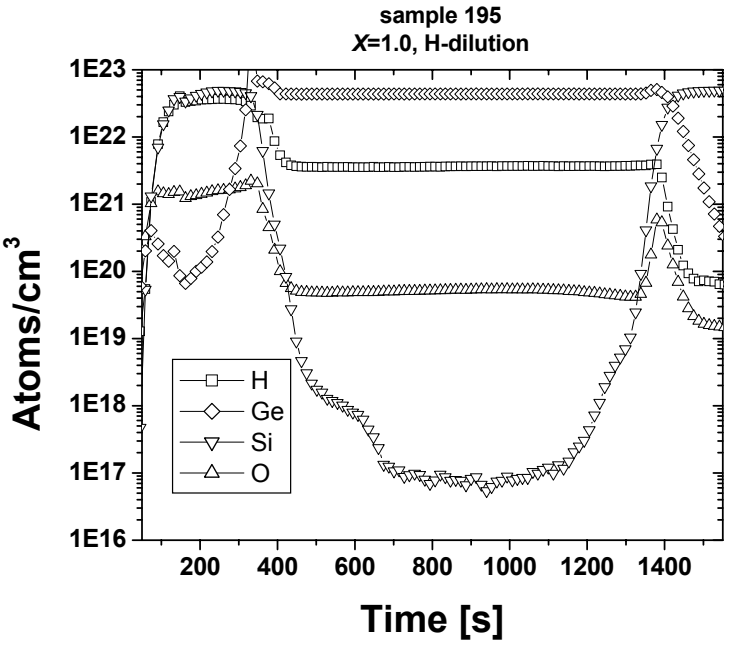
sample 195
X=1.0, H-dilution
Atoms/cm3
1E23
1E22
1E21
1E20
1E19
1E18
1E17
1E16
200
400
600
800
1000
1200
1400
Time [s]
H
Ge
Si
O

c)

Fig. 2

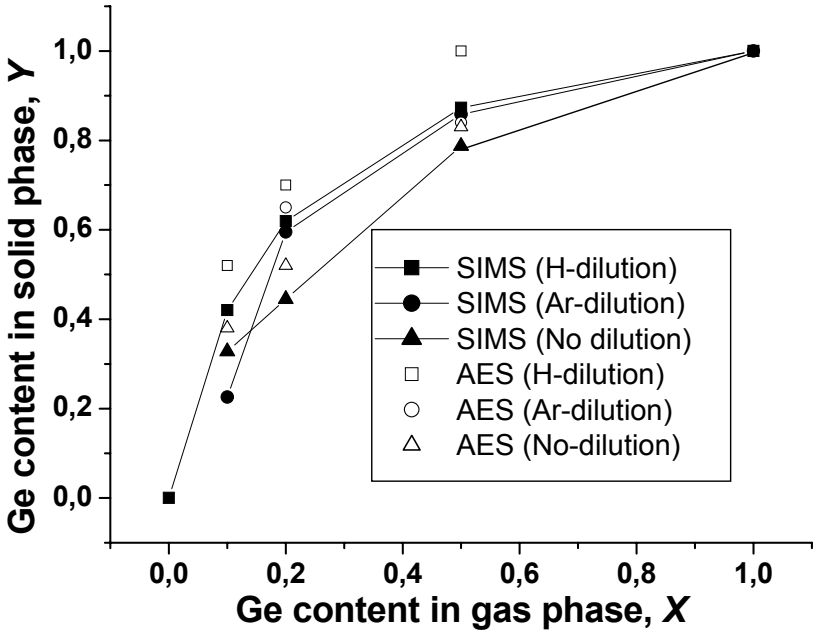
Ge content in solid phase, Y
Ge content in gas phase, X
1,0
0,8
0,6
0,4
0,2
0,0
0,0
0,2
0,4
0,6
0,8
1,0
SIMS (H-dilution)
SIMS (Ar-dilution)
SIMS (No dilution)
AES (H-dilution)
AES (Ar-dilution)
AES (No-dilution)

Fig. 3a

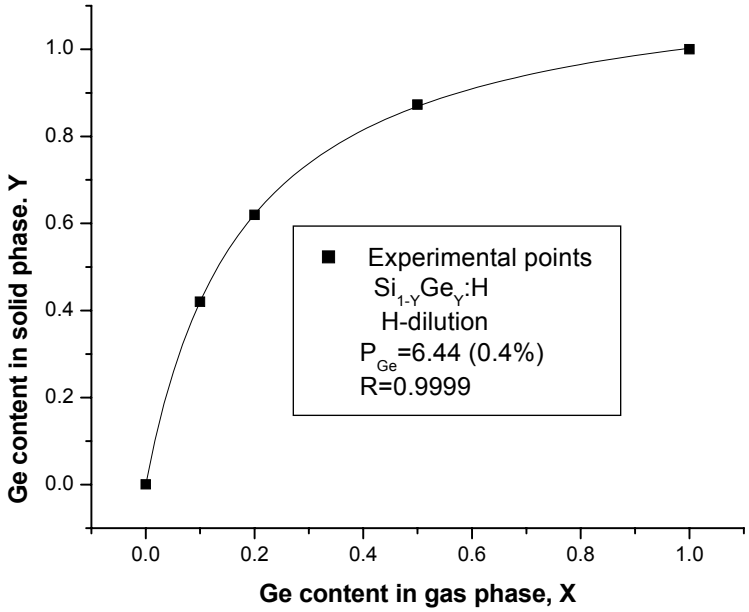
Ge content in solid phase, Y
Ge content in gas phase, X
1.0
0.8
0.6
0.4
0.2
0.0
0.0
0.2
0.4
0.6
0.8
1.0
Experimental points
Si1-YGeY:H
H-dilution
PGe=6.44 (0.4%)
R=0.9999

Fig.3b

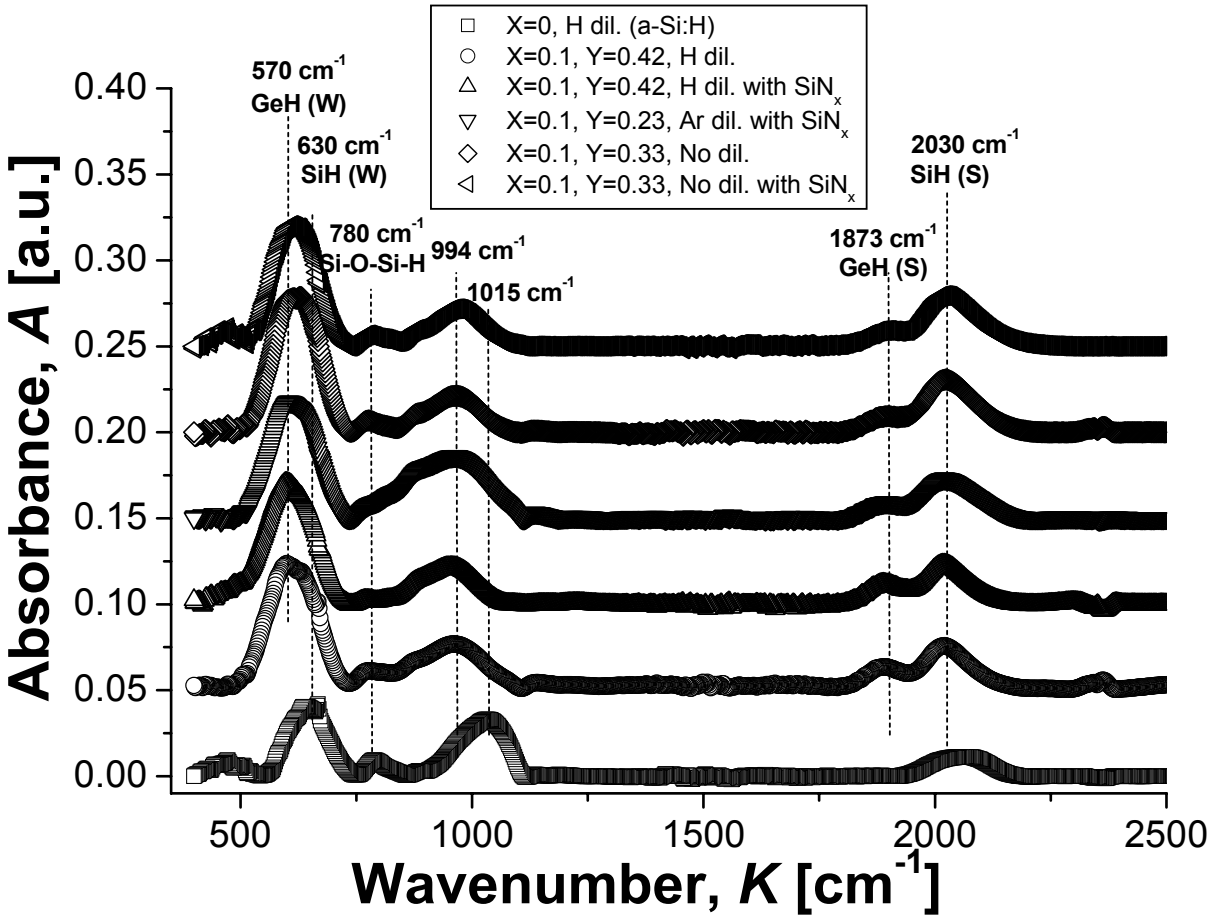
X=0, H dil. (a-Si:H)
X=0.1, Y=0.42, H dil.
X=0.1, Y=0.42, H dil. with SiNx
X=0.1, Y=0.23, Ar dil. with SiNx
X=0.1, Y=0.33, No dil.
X=0.1, Y=0.33, No dil. with SiNx
570 cm-1
GeH (W)
630 cm-1
SiH (W)
780 cm-1
Si-O-Si-H
994 cm-1
1015 cm-1
1873 cm-1
GeH (S)
2030 cm-1
SiH (S)
Absorbance, A [a.u.]
0.40
0.35
0.30
0.25
0.20
0.15
0.10
0.05
0.00
500
1000
1500
2000
2500
Wavenumber, K [cm-1]

Fig. 4a)

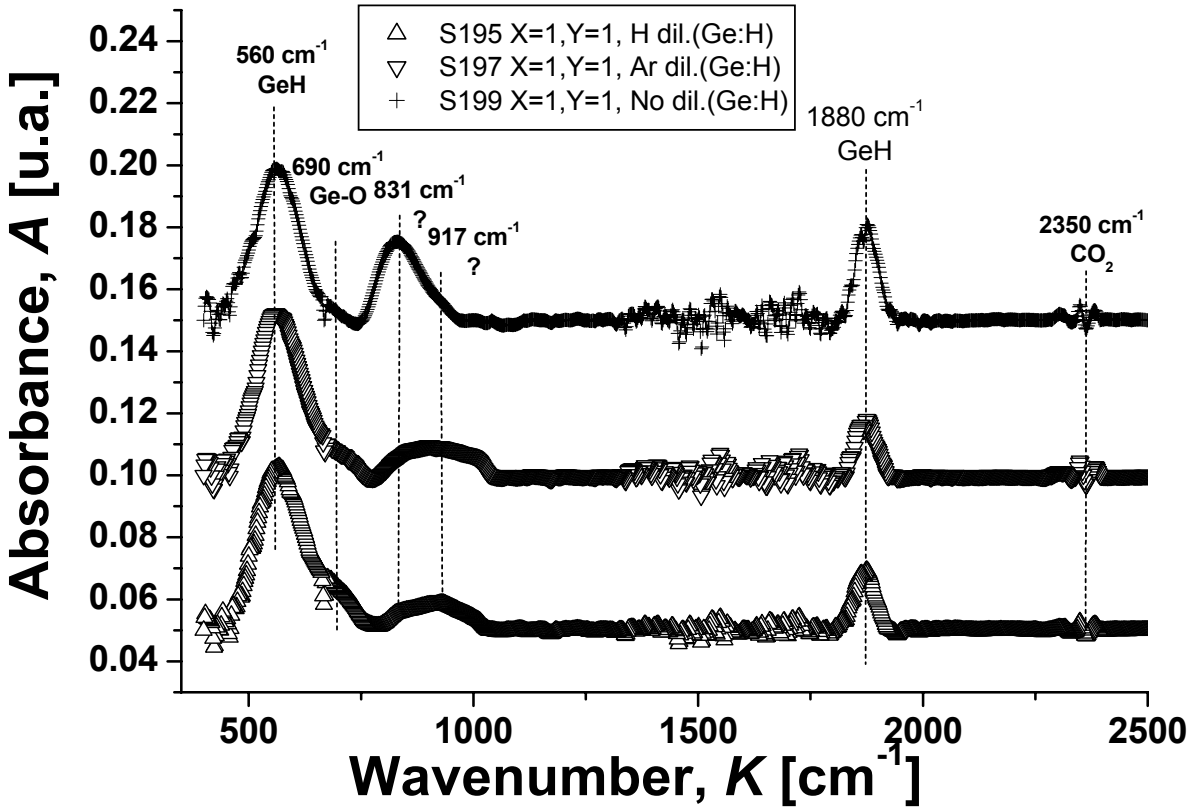
S195 X=1,Y=1, H dil.(Ge:H)
S197 X=1,Y=1, Ar dil.(Ge:H)
S199 X=1,Y=1, No dil.(Ge:H)
560 cm-1
GeH
690 cm-1
Ge-O
831 cm-1
?
917 cm-1
?
1880 cm-1
GeH
2350 cm-1
CO2
Absorbance, A [u.a.]
Wavenumber, K [cm-1]
0.24
0.22
0.20
0.18
0.16
0.14
0.12
0.10
0.08
0.06
0.04
500
1000
1500
2000
2500

b)

Fig. 4

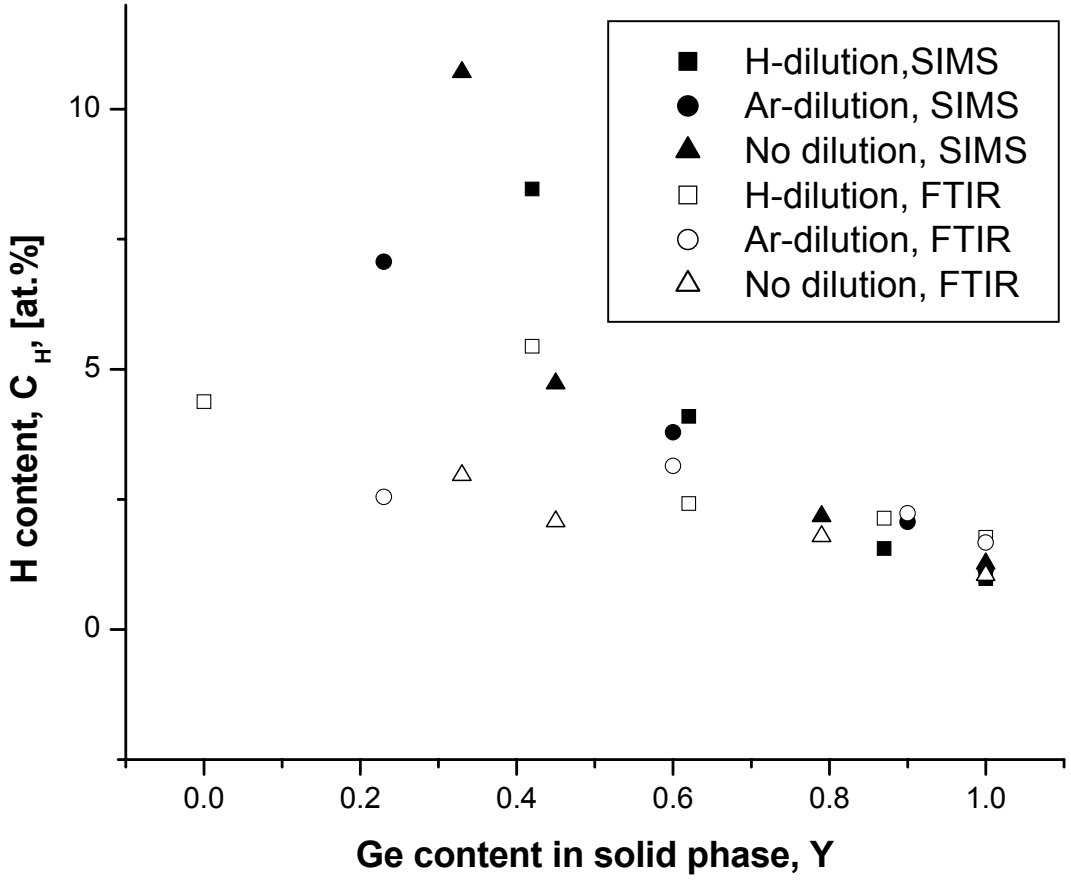
H-dilution,SIMS
Ar-dilution, SIMS
No dilution, SIMS
H-dilution, FTIR
Ar-dilution, FTIR
No dilution, FTIR
H content, C H, [at.%]
10
5
0
0.0
0.2
0.4
0.6
0.8
1.0
Ge content in solid phase, Y

Fig. 5.

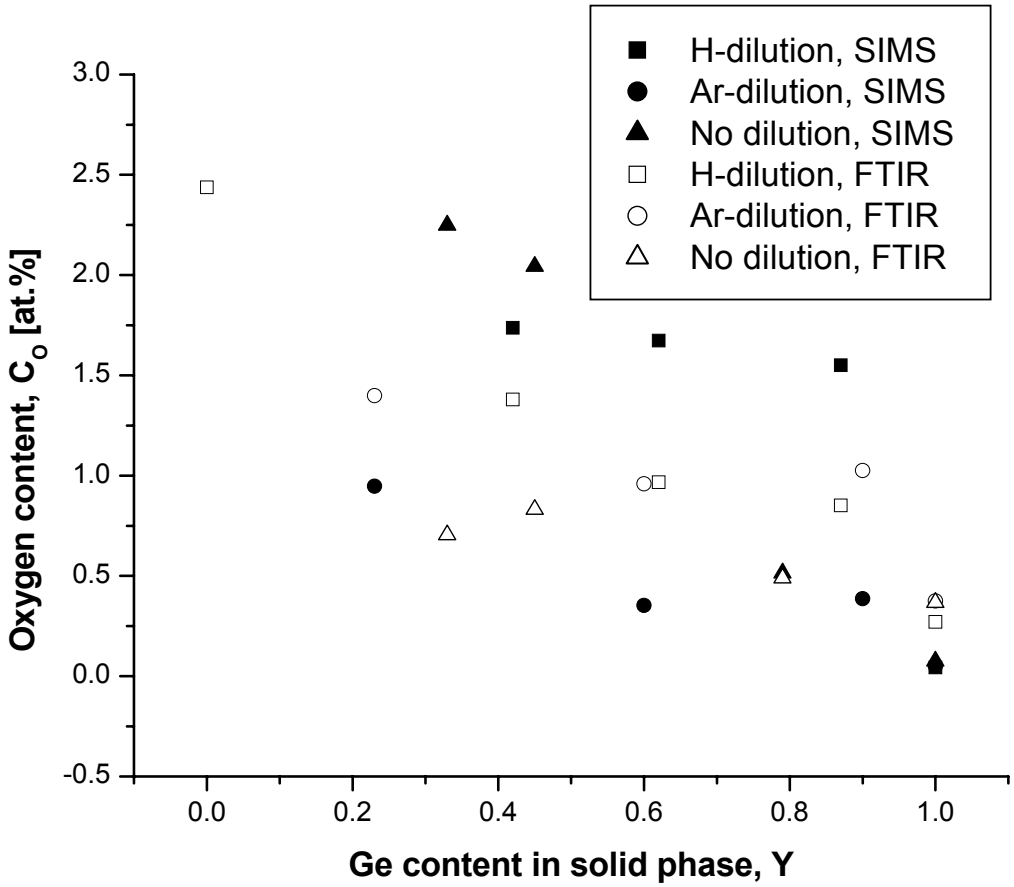
H-dilution, SIMS
Ar-dilution, SIMS
No dilution, SIMS
H-dilution, FTIR
Ar-dilution, FTIR
No dilution, FTIR
Oxygen content, C_o [at.%]
Ge content in solid phase, Y
3.0
2.5
2.0
1.5
1.0
0.5
0.0
-0.5
0.0
0.2
0.4
0.6
0.8
1.0

Fig. 6.

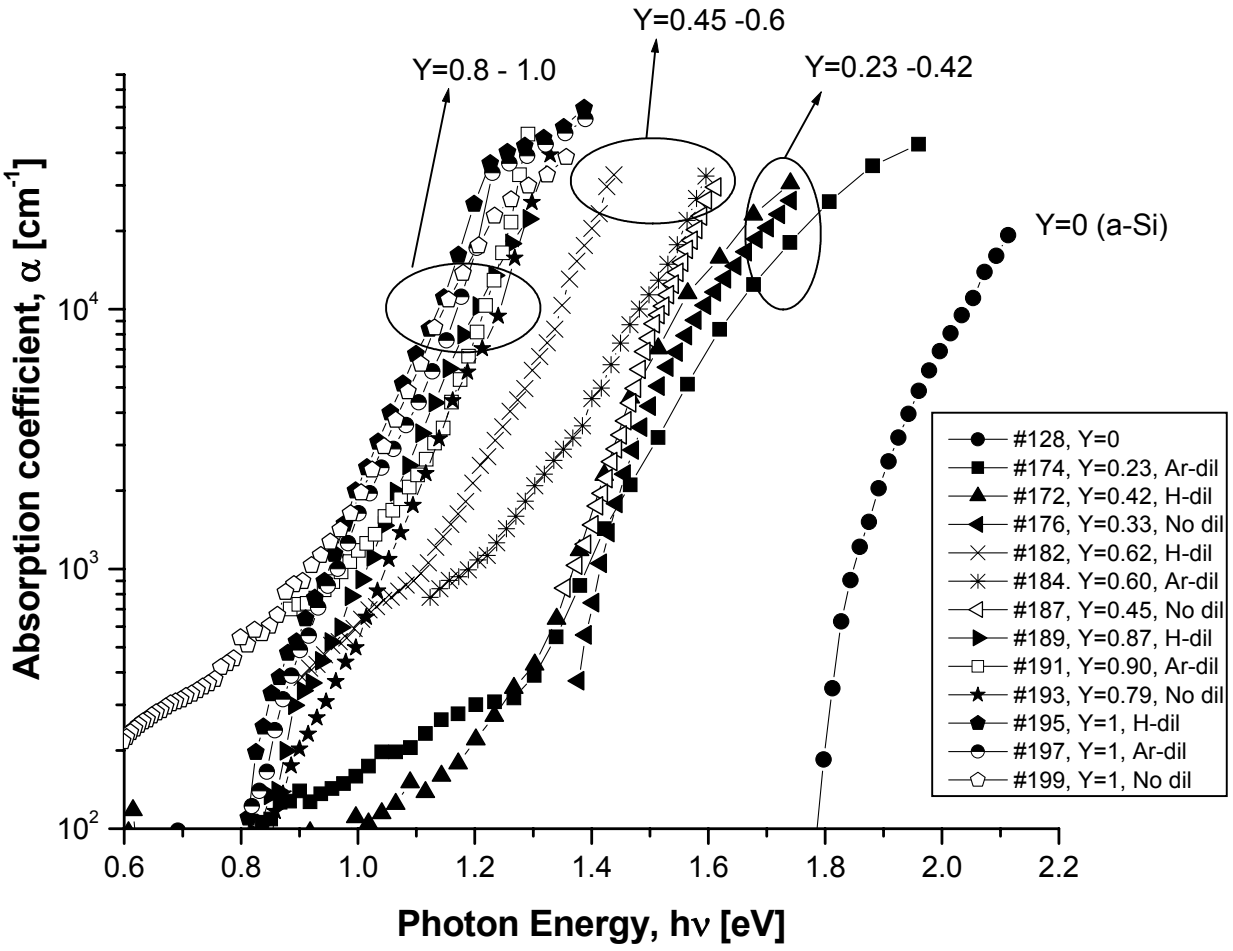
Y=0.45 -0.6
Y=0.8 - 1.0
Y=0.23 -0.42
Y=0 (a-Si)
Absorption coefficient, α [cm-1]
Photon Energy, hν [eV]
#128, Y=0
#174, Y=0.23, Ar-dil
#172, Y=0.42, H-dil
#176, Y=0.33, No dil
#182, Y=0.62, H-dil
#184. Y=0.60, Ar-dil
#187, Y=0.45, No dil
#189, Y=0.87, H-dil
#191, Y=0.90, Ar-dil
#193, Y=0.79, No dil
#195, Y=1, H-dil
#197, Y=1, Ar-dil
#199, Y=1, No dil

Fig. 7 a.

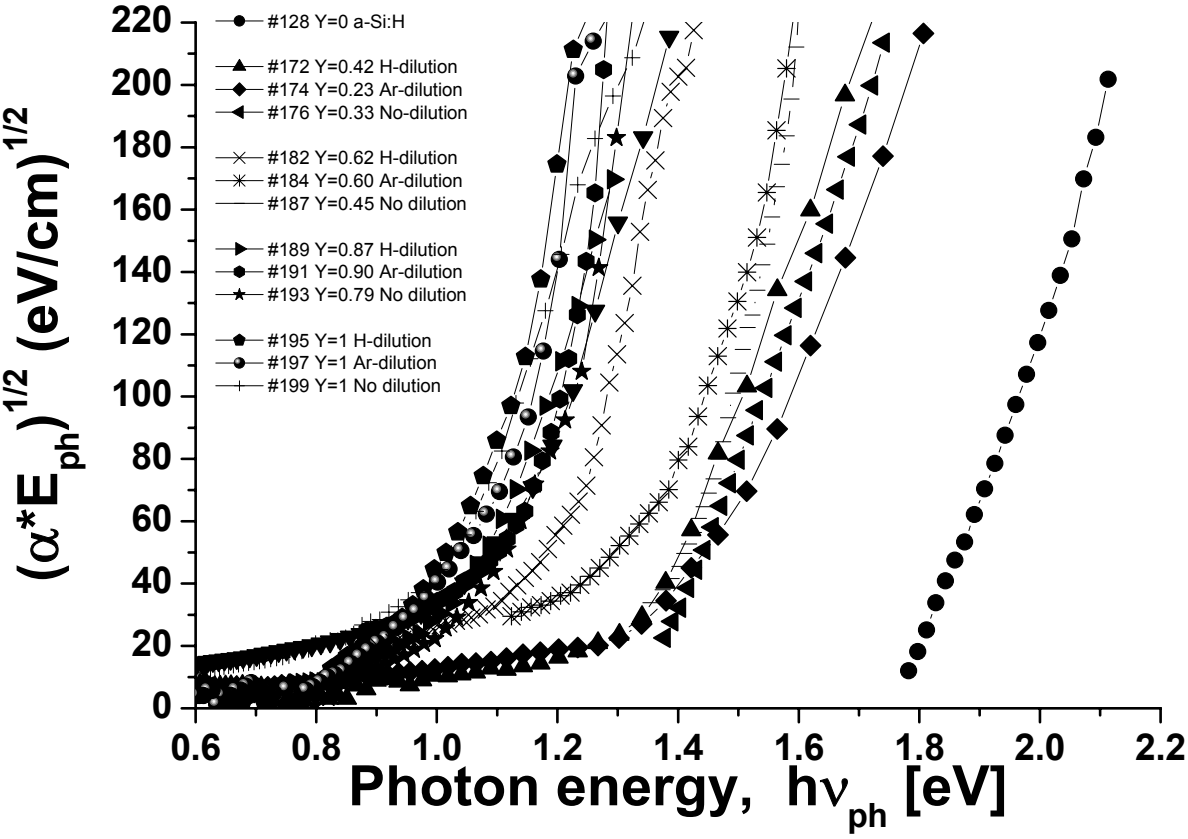
#128 Y=0 a-Si:H
#172 Y=0.42 H-dilution
#174 Y=0.23 Ar-dilution
#176 Y=0.33 No-dilution
#182 Y=0.62 H-dilution
#184 Y=0.60 Ar-dilution
#187 Y=0.45 No dilution
#189 Y=0.87 H-dilution
#191 Y=0.90 Ar-dilution
#193 Y=0.79 No dilution
#195 Y=1 H-dilution
#197 Y=1 Ar-dilution
#199 Y=1 No dilution
(α*E_ph)^1/2 (eV/cm)^1/2
Photon energy, hν_ph [eV]
0
20
40
60
80
100
120
140
160
180
200
220
0.6
0.8
1.0
1.2
1.4
1.6
1.8
2.0
2.2

Fig. 7 b)

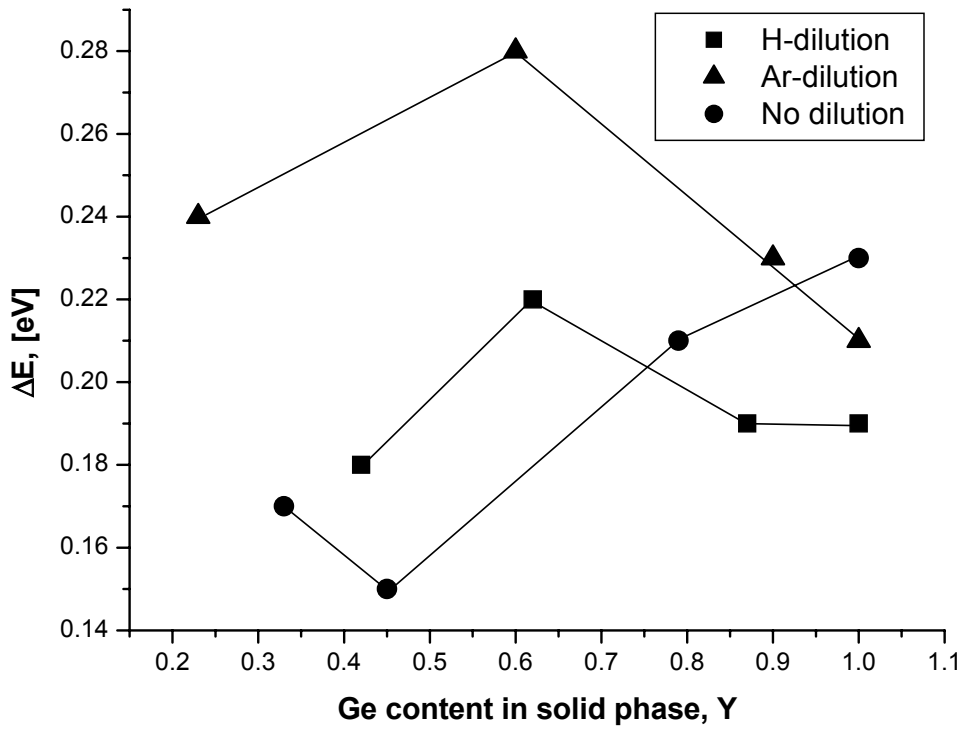
H-dilution
Ar-dilution
No dilution
ΔE, [eV]
0.14
0.16
0.18
0.20
0.22
0.24
0.26
0.28
0.2
0.3
0.4
0.5
0.6
0.7
0.8
0.9
1.0
1.1
Ge content in solid phase, Y

Fig. 8.

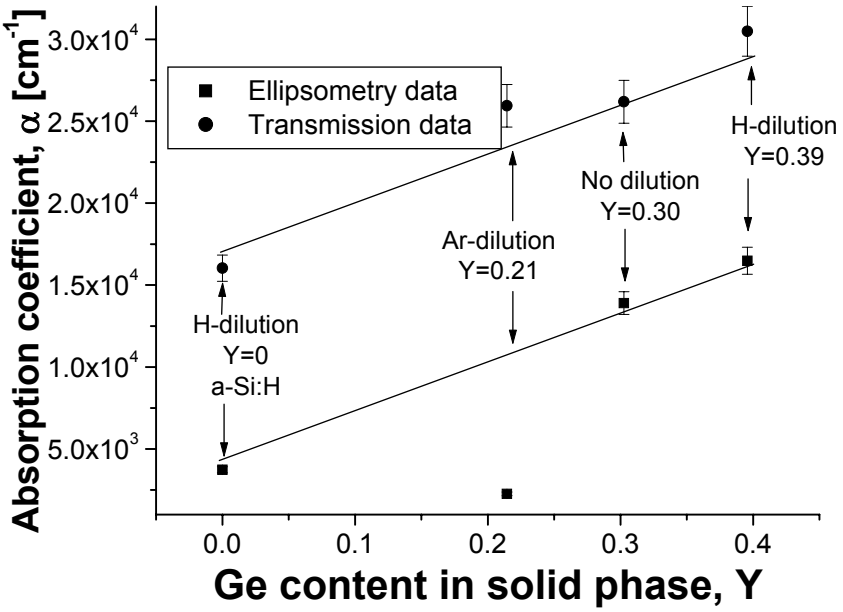
Absorption coefficient, α [cm-1]
3.0x10^4
2.5x10^4
2.0x10^4
1.5x10^4
1.0x10^4
5.0x10^3
Ellipsometry data
Transmission data
H-dilution
Y=0
a-Si:H
Ar-dilution
Y=0.21
No dilution
Y=0.30
H-dilution
Y=0.39
0.0
0.1
0.2
0.3
0.4
Ge content in solid phase, Y

Fig.9.

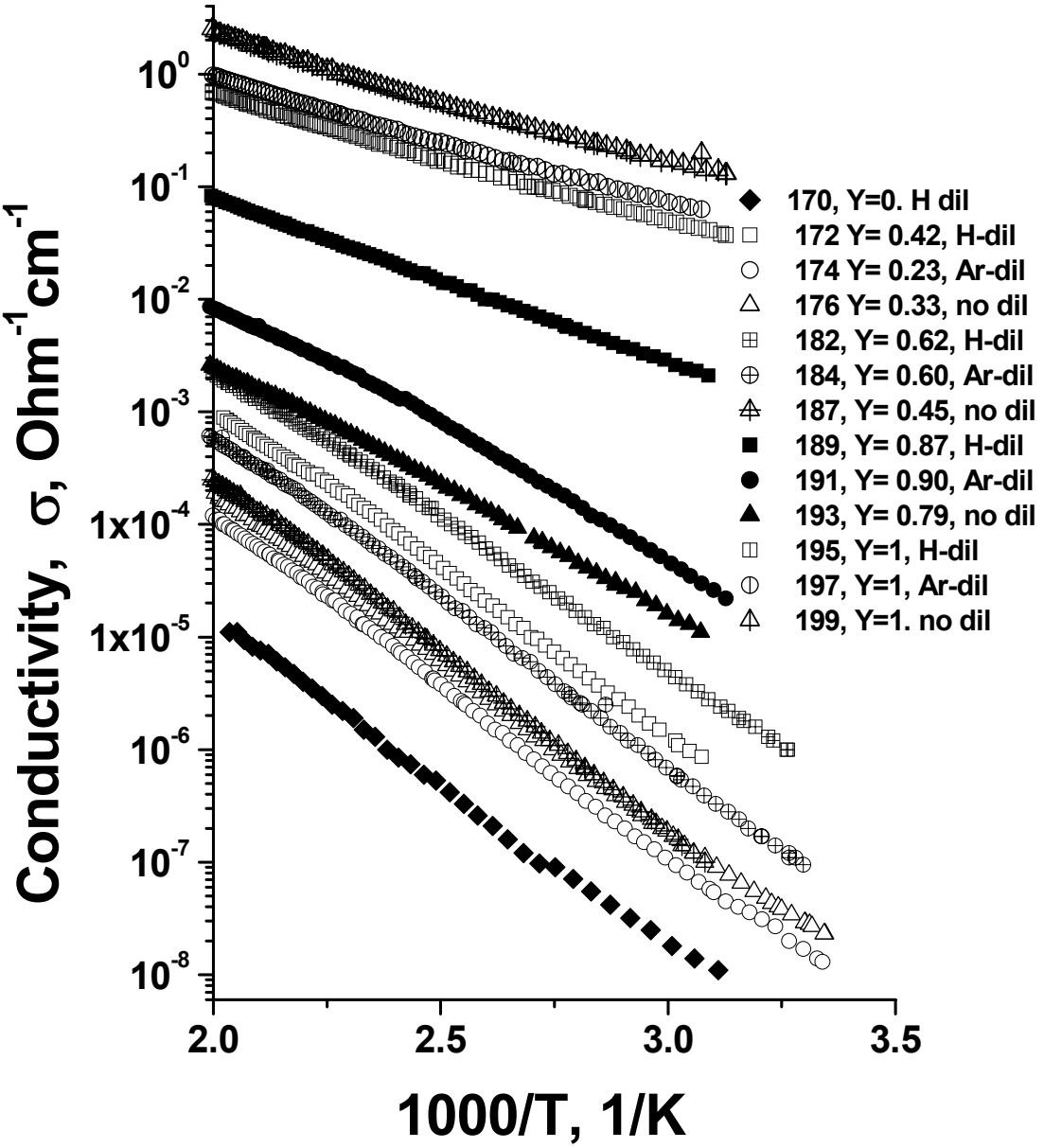
Conductivity, σ, Ohm-1cm-1
10^0
10^-1
10^-2
10^-3
1x10^-4
1x10^-5
10^-6
10^-7
10^-8
2.0
2.5
3.0
3.5
1000/T, 1/K
170, Y=0. H dil
172 Y= 0.42, H-dil
174 Y= 0.23, Ar-dil
176 Y= 0.33, no dil
182, Y= 0.62, H-dil
184, Y= 0.60, Ar-dil
187, Y= 0.45, no dil
189, Y= 0.87, H-dil
191, Y= 0.90, Ar-dil
193, Y= 0.79, no dil
195, Y=1, H-dil
197, Y=1, Ar-dil
199, Y=1. no dil

Fig. 10.

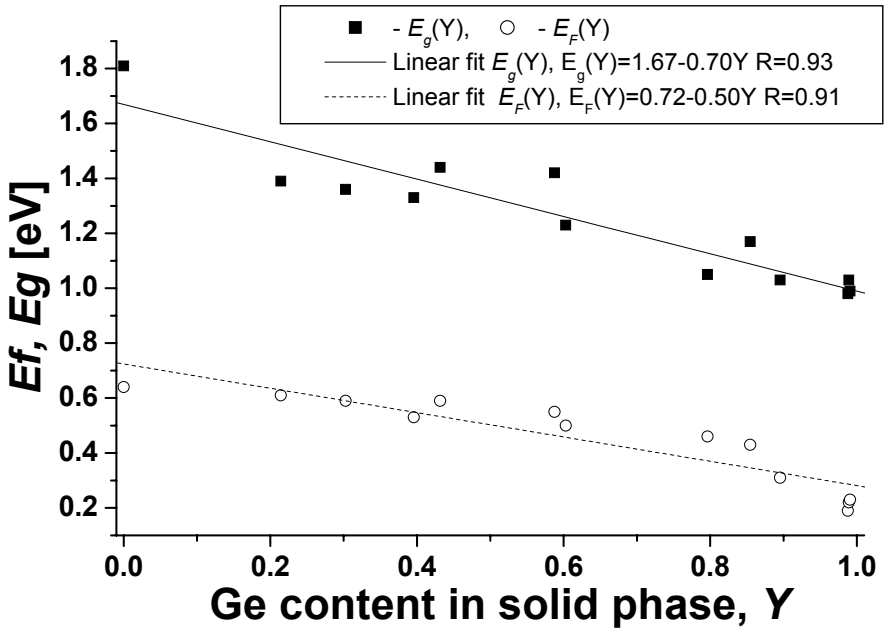
- E_g(Y), - E_F(Y)
Linear fit E_g(Y), E_g(Y)=1.67-0.70Y R=0.93
Linear fit E_F(Y), E_F(Y)=0.72-0.50Y R=0.91
Ef, Eg [eV]
1.8
1.6
1.4
1.2
1.0
0.8
0.6
0.4
0.2
0.0
0.2
0.4
0.6
0.8
1.0
Ge content in solid phase, Y

Fig. 11.

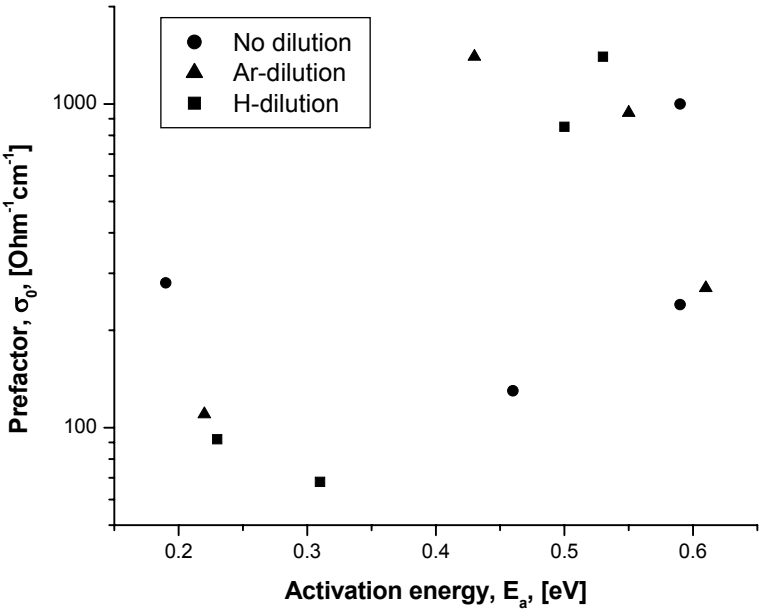
No dilution
Ar-dilution
H-dilution
1000
100
Prefactor, σ_0, [Ohm^{-1}cm^{-1}]
0.2
0.3
0.4
0.5
0.6
Activation energy, E_a, [eV]

a)

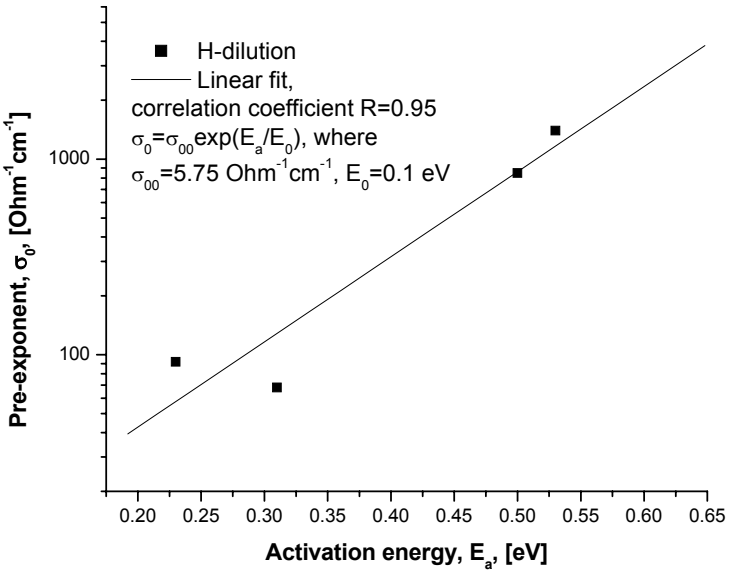
H-dilution
Linear fit,
correlation coefficient R=0.95
$\sigma_0=\sigma_{00}\exp(E_a/E_0)$, where
σ_{00}=5.75 Ohm^{-1}cm^{-1}, E_0=0.1 eV
1000
100
Pre-exponent, σ_0, [Ohm^{-1}cm^{-1}]
0.20
0.25
0.30
0.35
0.40
0.45
0.50
0.55
0.60
0.65
Activation energy, E_a, [eV]

b)

Fig. 12

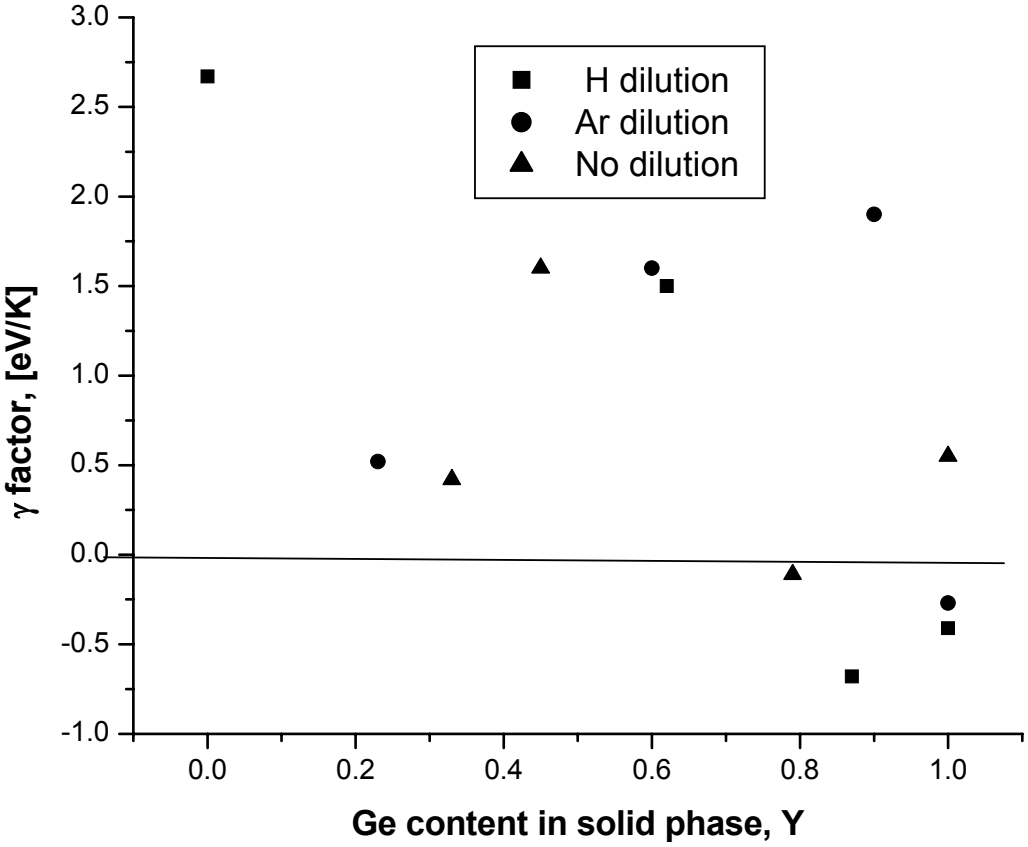
H dilution
Ar dilution
No dilution
γ factor, [eV/K]
Ge content in solid phase, Y
3.0
2.5
2.0
1.5
1.0
0.5
0.0
-0.5
-1.0
0.0
0.2
0.4
0.6
0.8
1.0

Fig. 13